

Reconstructing late Cenozoic deformation in central Panamint Valley, California: Evolution of slip partitioning in the Walker Lane

Joseph E. Andrew*

Alaska Division of Geological and Geophysical Surveys, Fairbanks, Alaska 99709, USA

J. Douglas Walker*

Department of Geology, University of Kansas, Lawrence, Kansas 66045, USA

ABSTRACT

New geologic mapping and Ar-Ar geochronology of the late Cenozoic volcanic-sedimentary units in central and southern Panamint Valley, California, provide the first known Miocene palinspastic reconstruction vectors for Panamint Valley. Panamint Valley contains active faulting and potentially accommodates a significant percentage of the slip of the Walker Lane at this latitude. Volcanism in Panamint Valley occurred during two time intervals, one ca. 15–13.5 Ma ago and a second ca. 4.5–4 Ma ago. The reconstruction vectors are based on unique relationships of sedimentary source areas and the only known Miocene intrusive zones to determine the displacement across Panamint Valley since ca. 15 Ma ago. The Argus Range was displaced ~17 km to the west-northwest, and the southern Slate Range was displaced 10.5 km to the north-northwest relative to the Panamint Range. Our displacement vector for reconstructing the past ~15 Ma of slip across Panamint Valley is 14 km shorter than previously published reconstruction models. We interpret this smaller slip value to be a function of the previous studies using displacement vectors that included a component of pre-15 Ma ago slip. The Harrisburg fault of the Tucki Mountain detachment system is a likely candidate for an earlier slip, possibly during the regionally observed extension during Late Cretaceous and Eocene. We created a model of the ca. 0–15 Ma ago displacement history of Panamint Valley using our new slip vectors and the slip vector for the Hunter Mountain fault. The Miocene exten-

sion begins with or slightly before ca. 15 Ma ago volcanism and may have continued to <~13.5 Ma ago. We interpreted the slip during Miocene extension to have occurred on one master detachment fault. Pliocene and younger extension is oblique to the Miocene extension, and the detachment fault was then cut up into discrete segments, the Emigrant, Panamint, and Slate Range detachment faults. The Panamint detachment was reactivated in an oblique normal sense, while slip on the other two detachment faults ceased; slip now occurs on nearby steeper normal faults. The Panamint detachment ends to the north and south in triple junctions: at the north end, slip is partitioned onto the Hunter Mountain and Towne Pass faults, and at the south end, slip is partitioned onto the Manly Pass and Southern Panamint Valley faults. The southern triple junction has an unstable geometry and it must migrate northward, lengthening the Southern Panamint Valley fault at the expense of the Panamint detachment. The continued slip on the unfavorably oriented low-angle Panamint detachment may be explained by the presence of weak fault gouge along it or by a regional pattern of slip partitioning. Major regional strike-slip faults, the Northern Death Valley and Garlock faults, are proximal to the northern and southern triple junctions. These two large faults may drag the two ends of the Panamint detachment with them, creating the triple junctions. The modern complex geometries and kinematics of Panamint Valley may therefore be a function of older structures being reactivated and interference with nearby faults.

INTRODUCTION

The study of large-magnitude, late Cenozoic extensional deformation of the central Basin and Range (Fig. 1) of the United States has illuminated the importance of extensional systems in deforming the continental lithosphere (e.g., Burchfiel and Stewart, 1966; Stewart, 1983; Wright, 1976; Wernicke, 1985; Wernicke et al., 1988; Snow and Wernicke, 1989, 2000). Current research in this area has focused on the active deformation in the western portion of the central Basin and Range referred to as the Walker Lane. The importance of the Walker Lane is that it accommodates ~25% of the Pacific–North American plate boundary motion, the remainder being taken up on the San Andreas Fault (Dokka and Travis, 1990; Dixon et al., 2000). Deformation in the Walker Lane is noted for its complex structural geometries, which are thought to be due in part to reactivation of earlier structures (Stewart, 1980; Oldow, 1992), and the relative immaturity of the fault system (Wesnousky, 2005).

Palinspastic reconstructions are an important tool for examining and understanding extensional deformation. Many studies have tried to reconstruct the displacement history of the fault-bounded range blocks in the central Basin and Range (e.g., Stewart, 1983; Wernicke et al., 1982, 1988; Prave and Wright, 1986; Snow and Wernicke, 1989, 2000; Serpa, 2000; Pavlis, 1996). The classic reconstruction study of Wernicke et al. (1988) interpreted the central Basin and Range to have been extended in excess of 250 km. A more detailed analysis by Snow and Wernicke (2000) derived space-time strain paths leading to 250–300 km of extension since 36 Ma ago. McQuarrie and Wernicke (2005) compiled

*Andrew: joseph.andrew@alaska.gov. Walker: jdwalker@ku.edu.

the existing reconstruction data from this region to create a time-integrated regional analysis of fault displacements since 36 Ma ago for the entire Basin and Range province. Their reconstruction for the central Basin and Range differs from that of Snow and Wernicke (2000) in some details, but is similar in the overall amount of Cenozoic extension. These values are significant to be able to evaluate the strain attributed to Miocene extension versus strain related to Pliocene–Holocene transtensional deformation.

The faults in the Panamint Valley area, California, in the western portion of the central Basin and Range (Fig. 1), are thought to accommodate ~35% of the strain of the Walker Lane (Lee et al., 2009). This area has a complex system of late Cenozoic faults (Walker et al., 2005), but the deformation history is not well known because there are no published data for time periods older than the Pliocene to link the Argus Range to the Panamint Range across Panamint Valley. Previously published displacement vectors for Miocene and older reconstruction of the Argus Range to the Panamint Range were derived via a circuit of displacement vectors from nearby areas resolved across Panamint Valley. The published late Cenozoic displacement vectors for the Argus Range relative to the

Panamint Range are quite variable: the vector of Snow and Wernicke (2000) is about twice the length of those from Serpa and Pavlis (1996) and McQuarrie and Wernicke (2005) (Fig. 2). Each of these reconstructions for Panamint Valley used different data sets; Snow and Wernicke (2000) used Paleozoic and Mesozoic thrusts along with younger structures, whereas Serpa and Pavlis (1996) and McQuarrie and Wernicke (2005) used interpreted offsets along various supposed Neogene and Quaternary faults.

The discrepancy between these studies may be due to the age of structures being reconstructed, with a larger displacement using dominantly Mesozoic structures and smaller displacement using Cenozoic structures. All three reconstructions are potentially correct, provided that an unknown or misidentified deformation event displaced these blocks between Mesozoic thrusting and Miocene time. The reconstructions of Snow and Wernicke (2000) and, to a lesser extent, McQuarrie and Wernicke (2005) violate some known geologic relationships in Panamint Valley. The Snow and Wernicke (2000) model reconstructs the Mesozoic bedrock of the Argus Range on top of large areas of Miocene volcanic rocks of the southern Panamint Range (Johnson, 1957; Wagner, 1988; Andrew, 2002), potentially

at the time that these Miocene rocks were being deposited and/or erupted (Fig. 2).

Another check on the robustness of the reconstructions is the accuracy of the restored geometry of pre-Cenozoic features. One prominent pre-Cenozoic feature of the southern Panamint Range is the Early Cretaceous Manly Peak pluton, a steep-sided, batholithic-scale intrusion (Fig. 2; Johnson, 1957; Wrucke et al., 1995; Andrew, 2002). The steep geometry, large structural relief (>2 km of relief on exposures), and scale (an outcrop area of >250 km² with possibly twice this much covered by Miocene volcanics and Quaternary alluvium; Wrucke et al., 1995) of this pluton indicate that it should have continued to higher structural levels than the present exposures, and thus the top portion of this body would likely occur in any overlapping hanging wall of the west-dipping detachment fault that exhumed the Panamint Range. The reconstruction models of Snow and Wernicke (2000) and McQuarrie and Wernicke (2005) both have rocks of the Argus Range overlapping the present-day exposures of the Manly Peak pluton of the southern Panamint Range (Figs. 2B, 2C); the Snow and Wernicke (2000) model locates the central Argus Range over the Manly Peak pluton. The extensive mapping and geochronologic work in the Argus and Slate Ranges do not show exposures or contact-metamorphic effects of a steep-sided Early Cretaceous batholithic-scale pluton (Moore, 1976; Dunne and Walker, 2004). The reconstruction model by Snow and Wernicke (2000) violates the expected Early Cretaceous geometric relationships of the Panamint Valley area, and it is either incorrect or there are post-early Cretaceous deformations that are not accounted for.

We present interpretations for Cenozoic deformation across the Panamint Valley area derived from new detailed geologic mapping, and from stratigraphic and geochronologic studies in the northern Slate Range, central Argus Range, and southern Panamint Range (area of Fig. 3). We use these data to determine displacement vectors across Panamint Valley. These vectors are used to construct a model of displacement history over the past 15 Ma to examine the changes in fault geometry and partitioning of slip with time. This work complements and integrates recent work in the region by Andrew (2002), Walker et al. (2005), Didericksen (2005), and Numelin et al. (2007a).

GEOLOGIC FRAMEWORK OF PANAMINT VALLEY

Late Cenozoic faults in Panamint Valley form a complex of strike-slip, normal, and oblique-normal faults (Fig. 3A; Hopper, 1947; Hall,

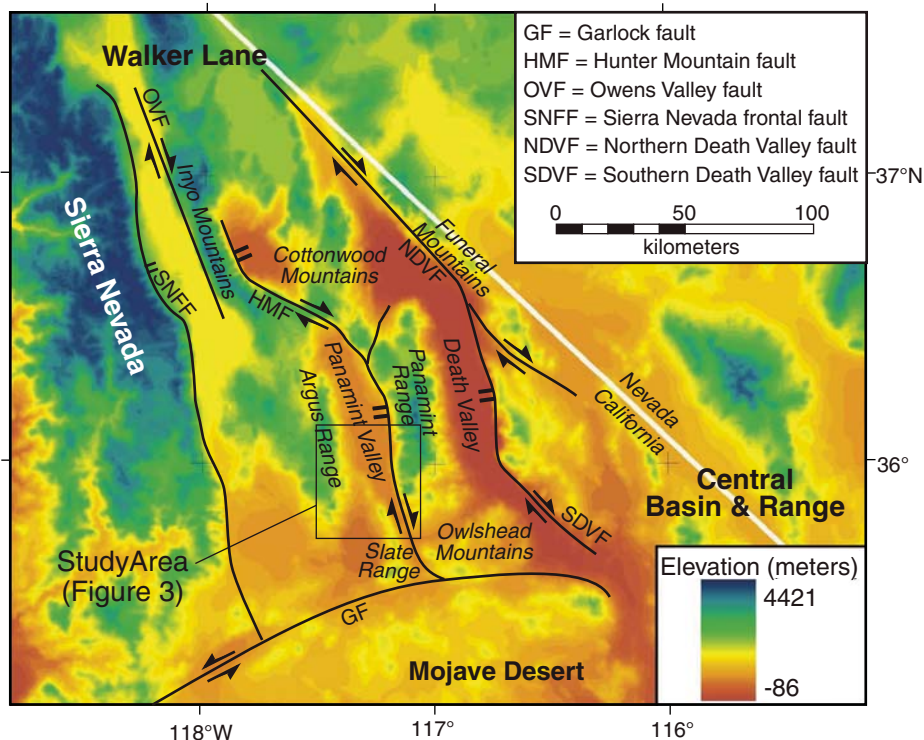


Figure 1. Overview map of the central Basin and Range, Walker Lane, major regional faults, and Panamint Valley region study area. Major or important faults for this study are shown by thick lines with strike-slip sense of shear indicated by sets of arrows and normal faults by double tick marks on the hanging-wall side.

Reconstructing late Cenozoic deformation in central Panamint Valley

1971; Smith et al., 1968; Smith, 1979; Burchfiel et al., 1987; Zhang et al., 1990; Densmore and Anderson, 1997; Walker et al., 2005). The west side of the Panamint Range is bound by a low-angle normal fault zone, the Panamint detachment (Cichanski, 2000; Kirby et al., 2004; Walker et al., 2005), which shows multiple overprinting fault striae directions (Andrew, 2002). Except for Holocene, locally stranded Pleistocene, and possibly some older sediments (Johnson, 1957), sediment filling Panamint Valley is in the hanging wall of this extensional fault. Two normal fault zones are exposed in the western portions of the central and southern Slate Range, i.e., the Searles Valley and Slate Range detachments (Fig. 3A; Walker et al., 2005; Didericksen, 2005; Numelin et al., 2007a). The northeast-striking, normal-oblique slip Manly Pass fault links the western Slate Range faults to the fault zone bounding the Panamint Range (Walker et al., 2005). The northern Slate Range and Argus Range are internally deformed by numerous relatively small offset normal, oblique, and strike-slip faults to create a

complex three-dimensional system of hanging-wall deformation (Walker et al., 2005).

Linking the Panamint Range to the Argus and Slate Ranges across Panamint Valley is problematic in that there are no pre-Cenozoic units common to the ranges on either side of the valley (Fig. 3B). The Argus and Slate Ranges have bedrock of Paleozoic–Jurassic metasedimentary rocks and Jurassic metovolcanics cut by Jurassic and Cretaceous intrusions (Moore, 1976; Fowler, 1982; Stone, 1985; Dunne and Walker, 1993, 2004). In contrast, the southern Panamint Range exposes Proterozoic gneiss, metasedimentary rocks, sills, and granitoids; early and late Paleozoic metasedimentary rocks; Triassic metasedimentary rocks; Jurassic metovolcanic and metasedimentary rocks; and Jurassic and Cretaceous intrusions (Johnson, 1957; Labotka et al., 1980; Cichanski, 1995; Andrew, 2002). The late Paleozoic rocks of the Slate and Argus Ranges have sedimentary and metamorphic facies distinctly different from the rocks in the Panamint Range (Johnson, 1957; Moore, 1976; Stone, 1985). The ages of the Jurassic metovol-

canic rocks and the ages, compositions, and textures of Mesozoic intrusions are distinctly different across Panamint Valley as well (for details on Mesozoic igneous units and their ages, see Johnson, 1957; Moore, 1976; Fowler, 1982; Cichanski, 1995; Mahood et al., 1996; Andrew, 2002; Dunne and Walker, 2004).

There are no pre-Cenozoic structures that definitively match across Panamint Valley. All of the adjacent ranges contain northward-trending Mesozoic thrust faults and folds (Moore, 1976; Fowler, 1982; Johnson, 1957; Cichanski, 1995; Andrew, 2002) and west-northwest-trending Late Jurassic dike swarms (Moore, 1976; Chen and Moore, 1979; Andrew, 2002), but there are no unique geometric, geochronologic, or stratigraphic ties to link these across Panamint Valley.

The only geologic units common to these ranges are Cenozoic volcanic and sedimentary rocks (Fig. 3A). Pliocene sediments and volcanics in the northern Panamint Valley have been examined (Hall, 1971; Schweig, 1989; Snyder and Hodges, 2000), and a set of reconstruction constraints has been published for Pliocene

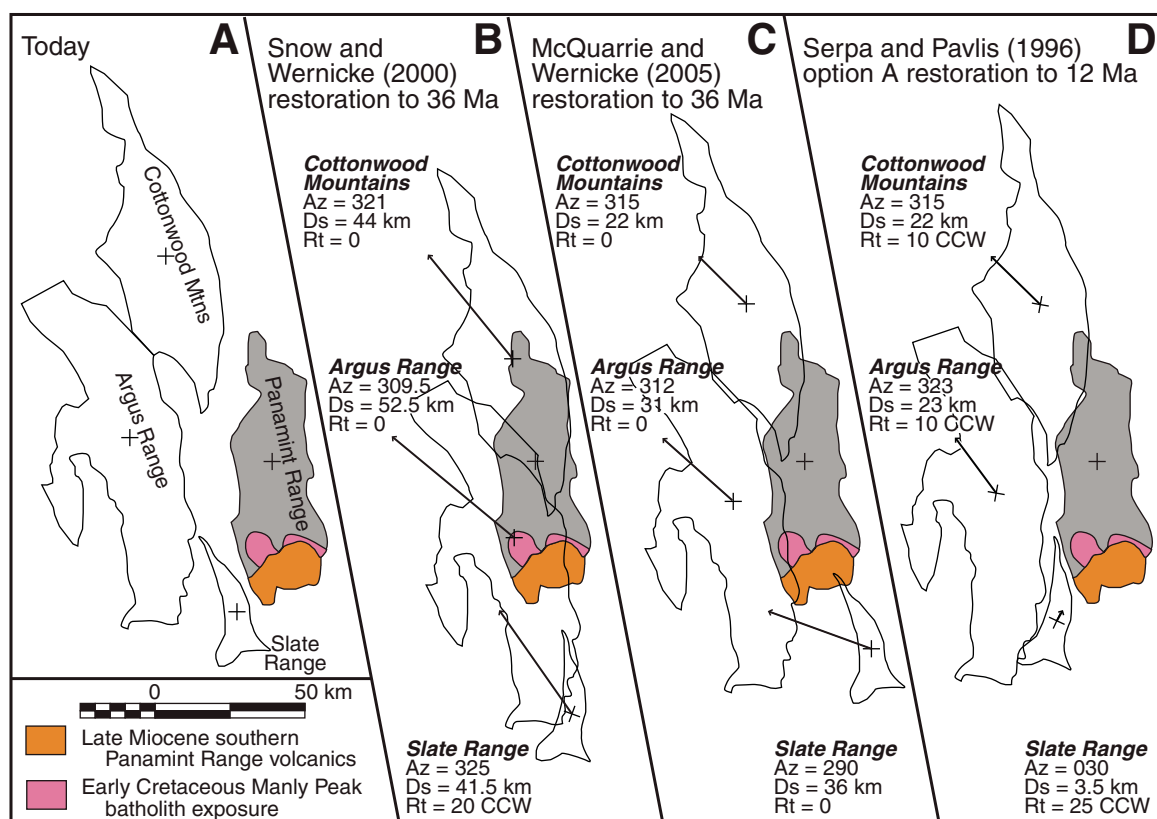


Figure 2. Published palinspastic reconstruction displacement vectors relative to the Panamint Range for the Panamint Valley region. (A) Current configuration of the ranges surrounding Panamint Valley. (B, C, D) Published displacement vectors for the Panamint Valley region. The arrow for each range indicates displacement vector (distance and azimuth, Ds, Az) of the center marker (+ symbol) with respect to the Panamint Range. Vertical axis rotations (Rt) are denoted by counterclockwise (CCW) displacement to the Panamint Range.

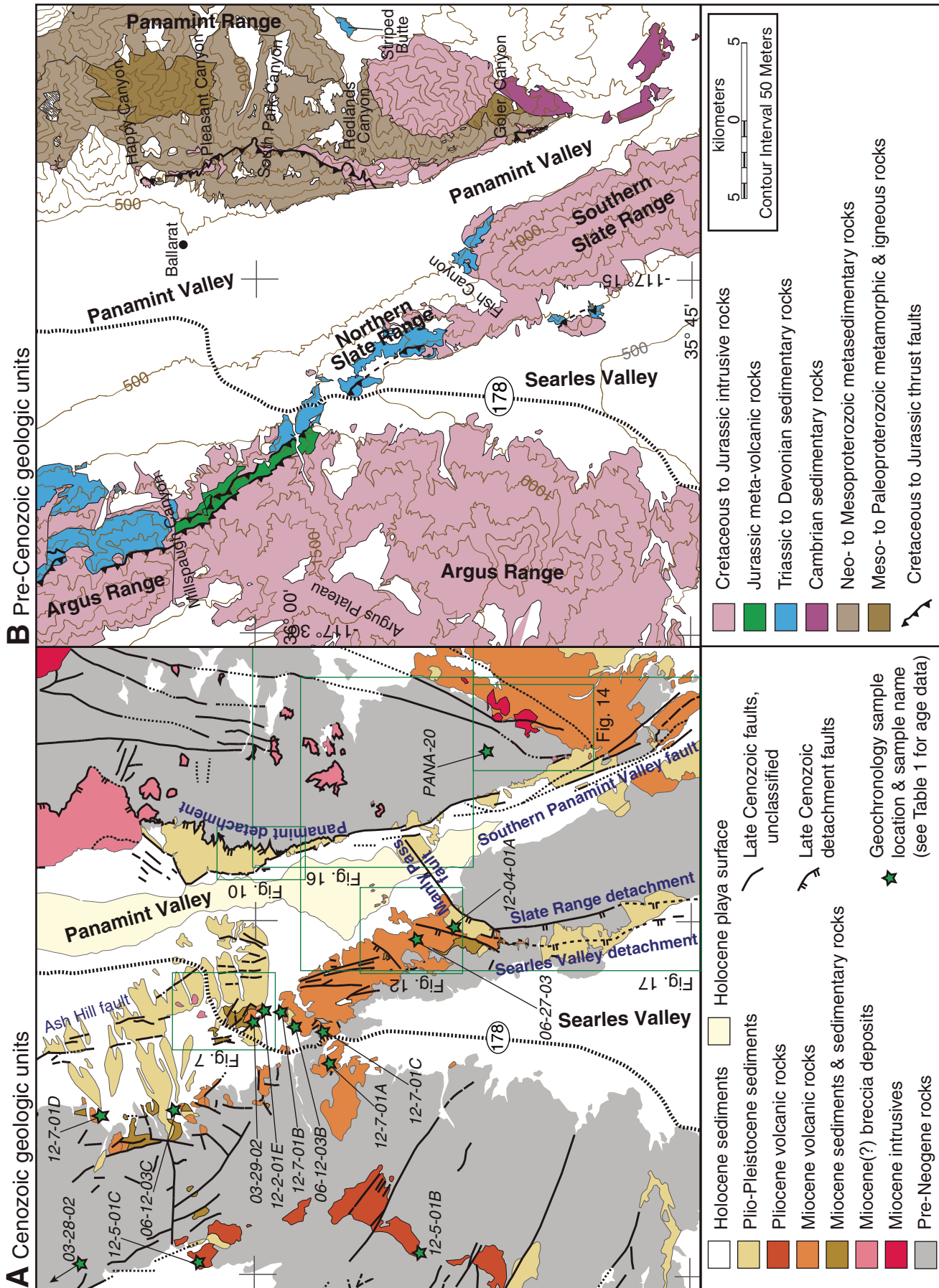


Figure 3. Simplified geologic maps of Panamint Valley region modified from Jennings et al. (1962), Walker et al. (2002), and Andrew (2002). (A) Cenozoic units and structures. (B) Pre-Cenozoic units and structures with reference localities mentioned in text.

basalts (Burchfiel et al., 1987). These Pliocene units do not record the Miocene deformation history of the Panamint Valley area (Hodges et al., 1990; Snow and Lux, 1999; Snyder and Hodges, 2000), although they may directly define the late Cenozoic history of the Hunter Mountain fault (Lee et al., 2009). The Cenozoic volcanic and interbedded sedimentary rocks in the central and southern portion of Panamint Valley were thought to be older than those present in northern Panamint Valley (Moore, 1976), but there were few existing geochronologic data for the southern area. Detailed examination of these Cenozoic units in central and southern Panamint Valley is crucial to our understanding of the Cenozoic deformation history of the Panamint Valley region and for palinspastic reconstruction of this deformation.

METHODS

The region around the central and southern Panamint Valley was mapped at 1:10,000 scale using the digital methods of Walker et al. (1996) and Walker and Black (2000) to examine Cenozoic deformation and find reconstruction piercing points or lines in either the pre-Cenozoic bedrock and structures or in Cenozoic volcanic and/or sedimentary rocks and sediments. This mapping built upon previous mapping of the three ranges surrounding Panamint Valley (Johnson, 1957; Smith et al., 1968, Smith, 1979; Moore, 1976; Albee et al., 1981; Fowler, 1982; Cichanski, 1995; Andrew, 2002; Didericksen, 2005). We collected samples for Ar-Ar age determinations (see Fig. 3A and Table 1 for locations). These were analyzed at the CLAIR facility at the Massachusetts Institute of Technology (MIT) and at the New Mexico Geochronology Research Laboratory: laboratory

descriptions can be found in House et al. (2002) and Brueseke et al. (2007), respectively. The interpreted age data are presented in Table 1 and Figure 4. Final age interpretations were made in consultation with K.V. Hodges (MIT) (2003, personal commun.) and M.T. Heizler (New Mexico Tech) (2005, personal commun.).

OBSERVATIONS

General Cenozoic Stratigraphic Framework

Cenozoic volcanic and sedimentary rocks mantle the ranges of the Panamint Valley region (Johnson, 1957; Moore, 1976; Smith et al., 1968; Fowler, 1982) (Fig. 3A). Although there is spatial variation in thickness and succession, there is a generally consistent stratigraphic order to these units (see generalized stratigraphic columns in Fig. 5). The following sections describe the Cenozoic rocks in the Panamint Valley region, and emphasize details of the volcanic-sedimentary sequence critical to our reconstruction of deformation.

The bases of the late Cenozoic sedimentary and/or volcanic sequence are arkoses and conglomerates (unit mTc in Fig. 5) deposited on an erosional unconformity. A possibly time-correlative rock unit (see following sections for further discussion) is a set of single clast-type breccia deposits (mTx in Fig. 5) exposed on the western slope of the central and southern Panamint Range and at one locality within Panamint Valley. These breccia deposits are not in contact with any other late Cenozoic deposits except Holocene alluvium, so their exact stratigraphic position is not known.

The earliest volcanic rocks are local basalt flows (unit mTbb in Fig. 5). Near Fish Canyon in

the Slate Range, these are overlain by rhyolitic lava flows and domes (unit mTr in Fig. 5), which occur above or are locally interbedded with the basal deposits. The first regionally persistent unit is a white felsic pumiceous deposit (unit mTp in Fig. 5). These oldest Cenozoic volcanic rocks are bimodal (basalt and felsic pyroclastic units), and define a period of activity ca. 15 Ma ago (Figs. 4K, 4L, 4M; Table 1). The main volcanic sequence overlies the pumiceous deposit, beginning with andesite and basaltic-andesite flows and associated debris-flow deposits (combined as unit mTba in Fig. 5), and including lesser amounts of interlayered basaltic lava. These intermediate to mafic volcanic rocks overlying the felsic pyroclastic layer have ages overlapping within error around from ~14 Ma old (Figs. 4D–4I; Table 1). Two localities in the southern part of the study area record relatively younger, slightly more felsic volcanism of rhyolitic to andesitic compositions (unit mTa in Fig. 5). Lava flows from a much younger episode of volcanism are recorded only in the high plateau of the Argus Range (Fig. 3; unit pTb in Fig. 5). These basalt flows are Pliocene; three samples give Ar-Ar plateau ages of 4.5–4.0 Ma old (Figs. 4A, 4B, 4C; Table 1).

Capping the volcanic section are locally preserved conglomerates and rock-avalanche deposits derived from the volcanic sequence and conglomerates derived from the footwalls of the detachment faults of the Panamint and southern Slate Ranges. A lacustrine limestone occurs locally in the Argus Range above the Pliocene basalts (unit pTl in Fig. 5; Moore, 1976). The Miocene sedimentary and volcanic rocks of the Argus and Slate Ranges and well-cemented older conglomerates exposed along the Panamint Range front are tilted ~30°–40° to the east and southeast (Fig. 6A). Pliocene basalts

TABLE 1. ⁴⁰AR/³⁹AR GEOCHRONOLOGY RESULTS

Sample	Material	Location	Easting	Northing	Age (Ma)
<u>Samples from Slate and Argus Ranges volcanic sequence</u>					
12-5-01C	gm	South Etcherson Valley, Argus Range	456242	3988168	4.04 ± 0.10
03-28-02	gm	Etcherson Valley, Argus Range	453445	3991789	4.40 ± 0.20
12-5-01B	gm	Birchum Spring, Argus Range	456075	3973608	4.50 ± 0.24
12-4-01A	gm	Fish Canyon, Slate Range	476683	3971074	12.81 ± 0.40
12-7-01B	gm	Northeast of old Slate Range Crossing Road	470424	3980567	13.12 ± 0.77
12-7-01D	bt	Eastern Argus Range	464236	3989505	13.35 ± 0.49
12-2-01E	gm	Panamint Valley Inselberg	471962	3983677	13.37 ± 0.60
12-7-01C	gm	Old Slate Range Crossing Road	470636	3980012	14.49 ± 0.86
06-12-03C	bt	Mouth of Millsbaugh Canyon, Argus Range	465457	3988775	13.49 ± 0.03
12-7-01A	gm	West of Slate Range Crossing	497937	3980460	13.56 ± 0.12
06-12-03B	bt	East of old Slate Range Crossing Road	471004	3980493	13.92 ± 0.06
03-29-02	gm	Panamint Valley Inselberg	470668	3985253	14.55 ± 1.16
06-27-03	gm	North of Fish Canyon, Slate Range	475552	3973177	13.79 ± 0.07
<u>Sample from the Panamint Range volcanic field</u>					
PANA-20	bt	Dike in Goler Canyon, Panamint Range	488545	3968691	13.41 ± 0.46

Note: Location in Universal Transverse Mercator, Zone 11N, Datum NAD83. Error on age is reported at the 95% level. bt—biotite; gm—groundmass.

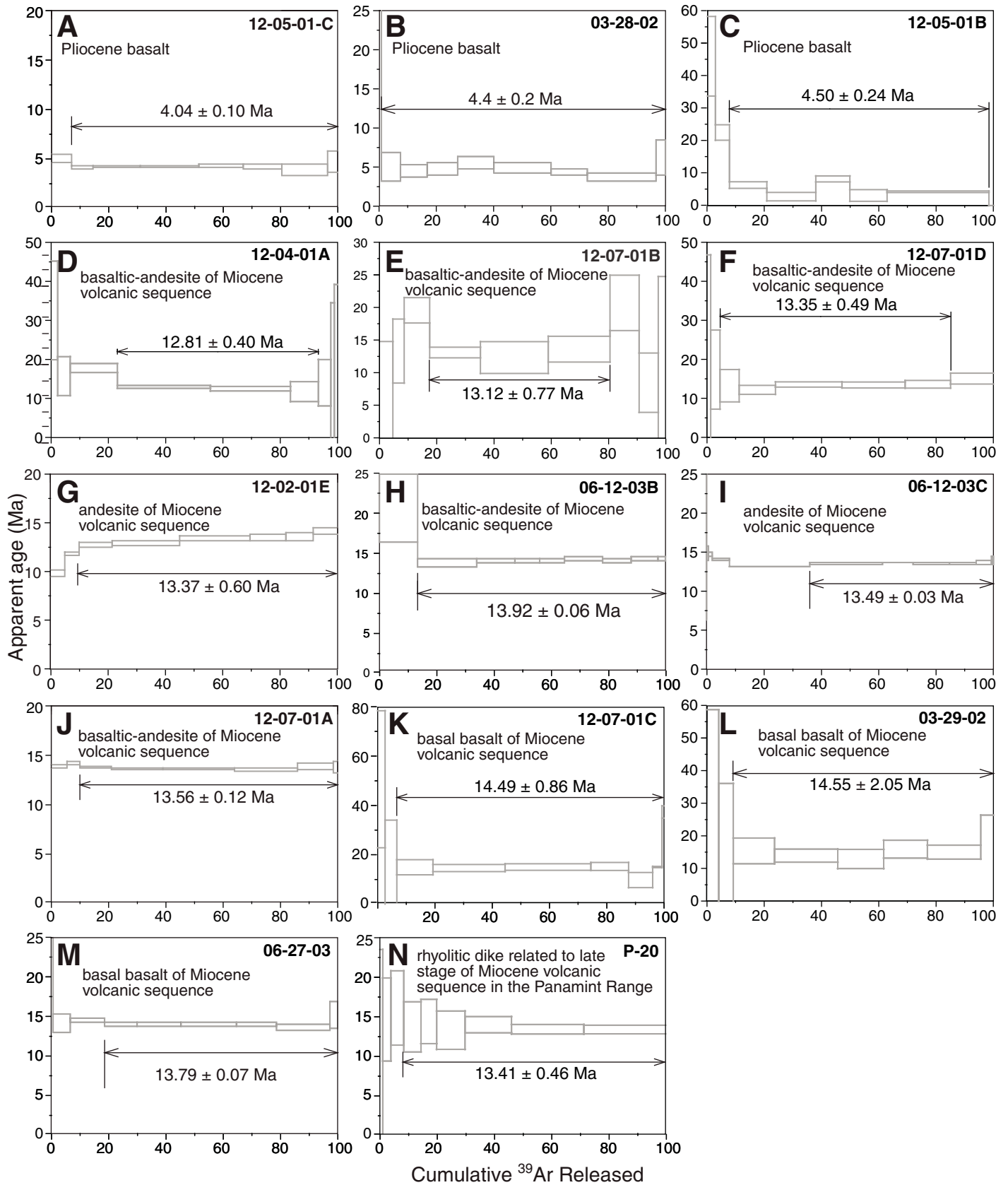


Figure 4. $^{40}\text{Ar}/^{39}\text{Ar}$ geochronology plots of plateau ages. See Table 1 for details and age interpretations for each sample. The $^{40}\text{Ar}/^{39}\text{Ar}$ data are included Supplemental Table 1.¹

¹If you are viewing the PDF of this paper or reading it offline, please visit <http://dx.doi.org/10.1130/GES00178.S1> or the full-text article at <http://geosphere.gsapubs.org> to view the supplemental table.

and Pliocene(?) and younger conglomerates along the Panamint Range front are generally slightly tilted, but can be steeply tilted within a few meters of faults (Fig. 6B). All of the rocks, including units as young as Holocene, are cut by faults (Fig. 3A; Smith et al., 1968; Smith, 1979; Zhang et al., 1990; Kirby et al., 2004).

Pertinent Details of Cenozoic Geologic Units

Miocene Conglomerate and Breccia Deposits at the Panamint Valley Inselbergs

A sequence of coarse sedimentary rocks (mTc at section IN in Fig. 5) occurs in several inselbergs within western Panamint Valley north of the Slate Range along Highway 178 (Figs. 3A and 7). These sedimentary rocks are interbedded with a 14.6 ± 1.2 Ma old basalt flow (Fig. 4L) and are overlain by a 13.4 ± 0.6 Ma old andesitic lava flow (Fig. 4G). Bedding is generally massive (Figs. 8A, 8B), but locally there are clasts with relatively planar aspect ratios weakly defining bedding.

This conglomerate is distinctive in that it has clasts of rock types that are not present in the other exposures of Miocene conglomerates. Exposures of Miocene conglomerates in the Argus and Slate Ranges (this unit was not found in the Panamint Range) are basal conglomerates that have locally derived clasts of medium-grained Mesozoic granitoid rocks, and lower greenschist-grade metamorphosed Paleozoic and Mesozoic sedimentary and volcanic units. These Miocene conglomerates of the western Panamint Valley area have rare exotic clasts of rounded large (to 1 m diameter) boulders of weathered volcanic rocks and quartzite that are only present in significant amounts at one locality (WS in Fig. 5).

The distinctively different clasts in the Miocene conglomerate at the Panamint Valley inselbergs consist of: (1) yellow-tan, coarse-grained metadolostone (Zn of Fig. 8); (2) greenish-gray-colored layered calc-silicate (Zj of Figs. 8A, 8B); (3) massive blue limestone (metamorphosed, but not coarse grained) with centimeter-scale white calcite ring shapes that are probably relicts of crinoid stems; (4) thinly laminated blue-gray marble with dark-colored argillite (Zksd of Fig. 8A); (5) metadiamicrite with very dark-colored matrix; (6) dark gray quartzite; (7) metapebble conglomerate of stretched quartz pebbles in very dark-colored matrix; (8) dark-colored argillite (Zk of Figs. 8A, 9B); and (9) two varieties of coarse-grained, porphyritic granitoids. The clast size at the inselbergs varies from a few centimeters to several meters. Granitoid clasts are generally subround and very coarse with clasts

to 5 m in diameter (Figs. 8A, 8B). The composition of the rock units present as clasts changes laterally: dark-colored metasiliciclastics dominate the clast compositions in the southern exposures (labeled A in Fig. 7), whereas the yellow metadolostone (labeled B in Fig. 7) is dominant in the northern exposures and the green calc-silicate clasts only occur there. The composition of the granitoid clasts also varies systematically: north of Highway 178 (labeled B in Fig. 7) are dominantly of grayish, porphyritic, biotite granodiorites (Ksp in Fig. 8A), some of which have augen gneiss fabrics; while at and south of Highway 178 (labeled A in Fig. 7) they are mostly massive, light-colored, porphyritic, hornblende-biotite quartz monzonite with distinctive very light pink potassium feldspar porphyrocrysts (Kmp in Fig. 8B). The clast assemblage of the Miocene conglomerate at the Panamint Valley inselbergs is notable because the active washes that surround these deposits (sourced from the Argus and Slate Ranges) do not carry any of these rock types (Moore, 1976).

Exposures of single rock-type breccia deposits of two compositions occur at several smaller inselbergs a few kilometers northeast of the inselbergs with Miocene conglomerates (Fig. 7). One set of these inselbergs is composed solely of coarse-grained, massive, yellow-white recrystallized metadolostone (labeled C in Fig. 7), and others have clasts of green-gray, metacalc-silicates laminated on a centimeter scale with gray silica-rich layers, all of which have a strong ductile deformation fabric (labeled D in Fig. 7; Fig. 8C). These breccia deposits could be interpreted as landslide deposits because they are unsorted and have cataclastic-like textures with relatively angular clasts. These breccia deposits are exposed only north of Highway 178 and are not in contact with any other Tertiary units, although they are exposed within ~500 m of the northern facies of the basal conglomerate described above (Fig. 7). The dip of the nearby Miocene conglomerates projects below these breccia deposits (Fig. 7), so these breccia deposits are probably younger than the Miocene volcanic rocks.

Breccia Deposits along the Western Flank of the Panamint Range

Breccia deposits occur along the axial and upper western flank of the southern Panamint Range (Fig. 3A; unit mTx in Fig. 5). They occur as isolated masses of jumbled angular clasts of Neoproterozoic bedrock units exposed nearby, separated by a planar structure from in-place, nonbrecciated rocks of the Panamint Range (Fig. 9A; Johnson, 1957; Albee et al., 1981; Cichanski, 1995; Andrew, 2002). This contact (Fig. 9B) has been interpreted as an extensional

fault, in part because of strong stratal omission of submember units from the top of the Kingston Peak Formation below these masses of dolomite clasts (Johnson, 1957; Albee et al., 1981; Cichanski, 1995; Andrew, 2002) and because of locally exposed deformation fabrics (Fig. 9B). These deposits are interpreted to be emplaced either by normal faulting or by mass wasting onto an exhumed normal fault surface (Cichanski, 1995).

The clast composition in the breccia deposits varies along the length of the Panamint Range. Exposures north of Happy Canyon (column HS in Fig. 5) have clasts of the dark metasiliciclastic rocks Kingston Peak Formation. The breccia deposits to the south are composed of clasts of light yellow, coarse-grained metadolostone (Figs. 9A, 9B, 9C) that is correlated to nearby outcrops of Noonday Dolomite. A few exposures of these southern breccia deposits (portions of column SB in Fig. 5) have gray-green laminated calc-silicate clasts correlated to the Johnnie Formation, and others have metaargillite laminated blue marble of the Sourdough Limestone Member of the Kingston Peak Formation (Fig. 9D). The deposits dominated by Noonday Dolomite and Johnnie Formation clasts are very similar to those exposed in the northern Panamint Valley inselbergs.

Conglomerates along the Western Flank of the Panamint Range

The late Cenozoic conglomerates along the western flank of the Panamint Range do not have clast types similar to those found at the Panamint Valley inselbergs or in the basal conglomerates of the Argus and Slate Ranges. At least three sets of distinct conglomerates can be seen along the detachment fault bounding the western Panamint Range (Fig. 10). The oldest conglomerate (pmTc in Fig. 5) is strongly deformed and tilted, and is in fault contact with an underlying low-angle fault gouge zone (Figs. 10 and 11A). Strong calcite and silica cementation is notable in this unit. A second set of coarse clastic rocks overlies these rocks along an angular unconformity (Fig. 11B). These intermediate-age sediments (pTc in Fig. 5) have low eastward to subhorizontal dips and are poorly cemented. This unit was deposited directly onto the fault surface, fault gouge, and the older strongly deformed sediments (Figs. 11B, 11C). These intermediate units are cut by numerous other faults and local clastic dikes, and are strongly tilted and deformed only adjacent (to 2 m away) to faults. The faults cutting these intermediate-age units range from normal to strike slip and were not observed to cut the footwall rocks of the Panamint detachment. Near the ghost town of Ballarat, a reworked ash layer correlative with

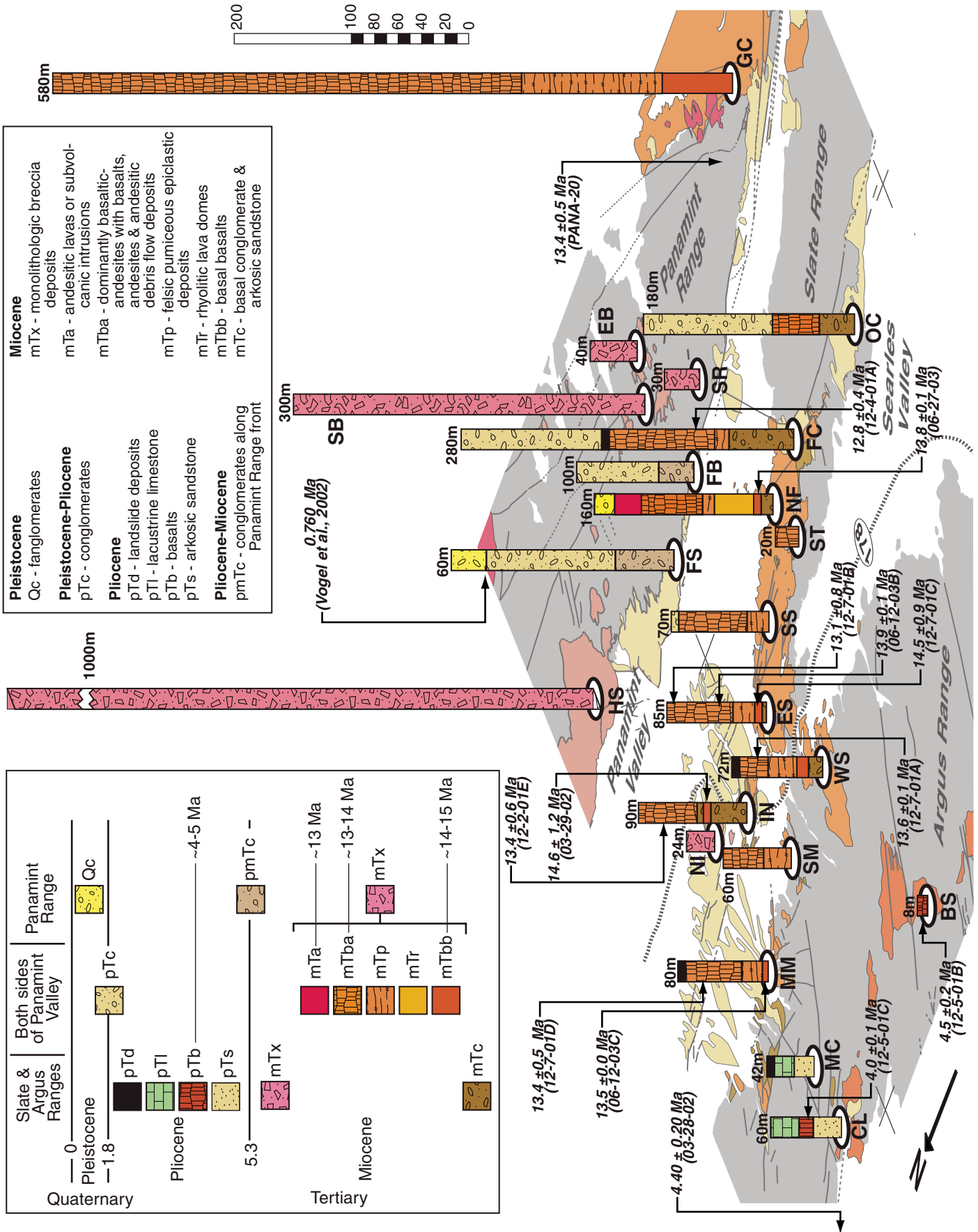


Figure 5. Simplified stratigraphic sections of Cenozoic rocks and deposits across the Panamint Valley region. The background is an oblique view of Figure 3A. Each section has a site label at the bottom and a cumulative thickness (in meters) labeled near the top. The location of each stratigraphic section is the ellipse shown at the bottom of each section. The geologic unit symbols are arranged graphically in relative chronological order separated into their occurrence area. For details, see text discussion on stratigraphy. The data in italics are age data and sample number placed, where possible, in the generalized stratigraphic columns. Stratigraphic section abbreviations: BS—Birchum Spring; CL—Carricut Lake; EB—Big Horn–Redlands Canyons divide; ES—east of Slate Range Crossing; FB—front of Big Horn Canyon; FC—Fish Canyon; FS—front of South Park Canyon; GC—eastern Goler Canyon; HS—Happy-Surprise Canyons divide; IN—Panamint Valley inselberg; MC—Millspaugh Canyon; MM—mouth of Millspaugh Canyon; NF—north of Fish Canyon; NI—northeastern Panamint Valley inselbergs; OC—Ophir Canyon; SB—South Park–Big Horn Canyons divide; SM—Sea Silica Mine; SR—south of Redlands Canyon; SS—southeast of Slate Range Crossing; ST—Slate Range Tower; and WS—west of Slate Range Crossing.

the Bishop tuff (U-Pb zircon ages ~ 760 ka old; Vogel et al., 2002) occurs within a thick section (>100 m) of coarse sediments that are deeply incised and unconformably overlie strongly deformed, well-cemented coarse sediments in fault contact with fault gouge. Thus, these intermediate-age sediments are in part as young as Pleistocene, while the strongly deformed sediments on the gouge zone are significantly older. The strongly cemented and deformed conglomerates have tilts similar to those of Miocene volcanic and sedimentary rocks in the Argus and Slate Ranges (Fig. 6A). The youngest set of sediments (Qc in Fig. 5) is relatively unfaulked, weakly incised, and does not show effects of Pleistocene pluvial reworking (Smith, 1979).

The conglomerate deposits along the Panamint Range front, from Pleasant Canyon to just south of Redlands Canyon (Fig. 10), are dominated by conglomerate clasts of Mesoproterozoic quartz-feldspar gneiss and metadiabase, which are the rock types that dominate the bedrock exposures along this portion of the range front. These clasts are generally coarse, from a few centimeters to 1–2 m in diameter, with generally coarser clasts of Mesozoic granitoids. The sources for the granitoid clasts are granitoid bodies exposed near the top of the steep range front (Fig. 3B). Other rock types are rare as clast types in the conglomerates between Pleasant and Redlands Canyons. Quaternary alluvial

fans have clasts similar to those in the older conglomerates. Holocene debris flows along the steep, fault-controlled range front have deposited boulders as much as ~ 2 km away from the range front. The coarsest boulders on the active alluvial fan surfaces are of Mesozoic granitoid compositions. None of the conglomerates along the western Panamint Range contains Miocene or Pliocene volcanic rocks.

Miocene Volcanic Section in Fish Canyon Area of the Northern Slate Range

The Miocene volcanic sequence in the Argus Range and northern Slate Range thickens to the southeast (Fig. 5). The thickest sections occur near Fish Canyon (column FC in Fig. 5) and have at least eight flow units, whereas within a few kilometers to the west there is only one lava flow unit (cf. columns ST, NF, and FC in Fig. 5). The sequence also thins to the north from Fish Canyon, but this decrease in thickness takes place over ~ 20 – 25 km (Fig. 5), indicating a north-south basin geometry for this sequence. The Fish Canyon area also contains the only intrusive and near-vent facies Miocene volcanic rocks in the Argus Range and northern Slate Range. A few kilometers to the north of Fish Canyon are several exposures of rhyolite domes within the basal portions of the volcanic section (Fig. 12) that overlie a 13.8 Ma old basal basalt flow and are underneath felsic pyroclastic

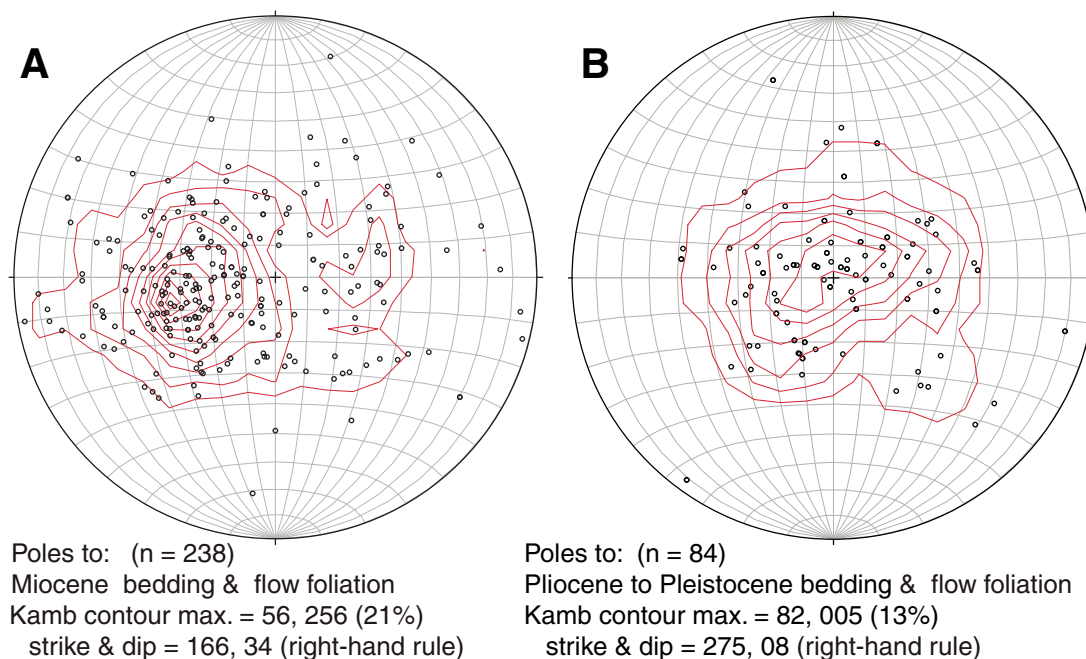


Figure 6. Equal-area stereograms for the Panamint Valley area. (A) Poles to bedding and volcanic flow foliation for Miocene units. Note the maxima of west-southwest-oriented poles, indicating an east-northeast tilt of $\sim 34^\circ$. (B) Poles to bedding and volcanic flow foliation for Pliocene–Pleistocene units. Note the overall subhorizontal maximum of bedding, with scatter due to local (a few meters) drag along faults cutting these units.

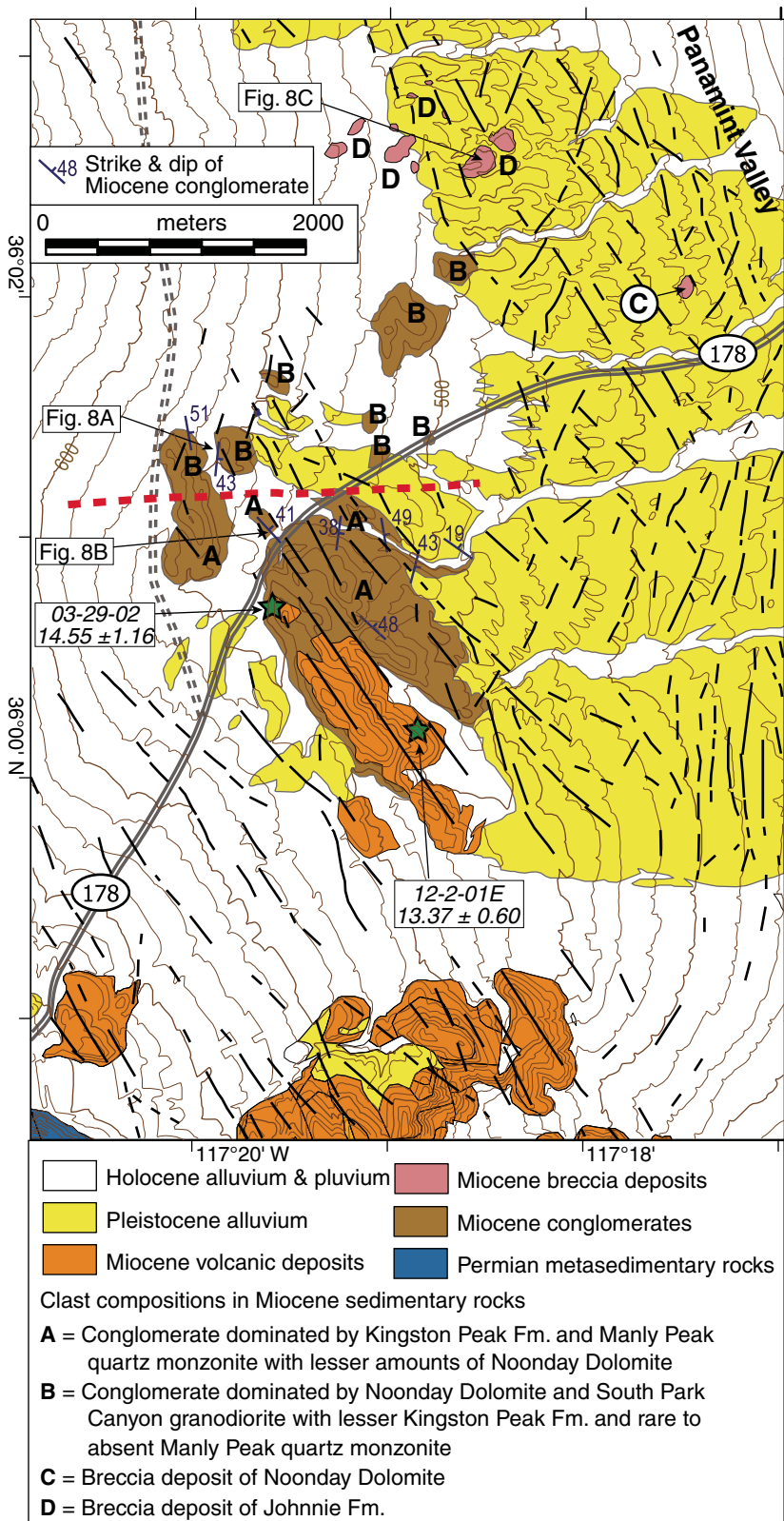


Figure 7. Detailed geologic maps of Miocene and younger deposits at the Panamint Valley inselbergs (see Fig. 3A for location). The clast compositions of each of the sedimentary and monolithic breccia deposits are denoted by A, B, C, or D. Red dashed line is the boundary of the northern and southern clast composition facies for the conglomerates.

deposits and voluminous basaltic-andesite lava flows. An agglomerate cone in Fish Canyon that is stratigraphically above the felsic pyroclastic unit is cut by a northeast-striking 12.5 Ma old basaltic intrusion that grades into a lava flow, which overflowed above and beyond the vent facies (Fig. 13A). Another set of probable near-vent volcanics occurs to the northeast of Fish Canyon as a series of anomalous steep-sided hills forming a linear trend out into the Panamint Valley playa (unit mTa in Fig. 12; Fig. 13B). These hills are of generally massive, aphanitic porphyritic igneous rock, but are extensively weathered, making classification difficult. Color indices indicate that most of these are andesitic in composition, with one set being more felsic (Fig. 12). The extreme weathering may be due to interactions with the saline waters of lakes that occupied Panamint Valley during the Pleistocene.

Miocene Volcanic Section in Goler Canyon Area of the Southwestern Panamint Range

The Miocene volcanic section in the Goler Canyon area (Figs. 14 and 15) is similar to that of the southern portion of the northern Slate Range in that there is a similar stratigraphy of volcanic units and there are also several intrusive units present (Johnson, 1957). The major difference is that the Goler Canyon volcanic sequence is at least twice as thick as the thickest portion of the volcanic rocks exposed in the Slate Range (cf. column GC with FC in Fig. 5). Mafic dikes intrude at least the lower and middle portion of the volcanic section in the southwestern Panamint Range, cutting the basal basalts and felsic pyroclastic unit and possibly the basaltic andesite sequence. A series of andesitic stocks and one rhyolitic stock cut the volcanic section and form a chain of intrusions starting just south of Goler Canyon and continuing northeastward for at least 6 km (Figs. 3A and 14). A rhyolitic dike strikes northwestward from the intersection point of the mafic dikes with the andesitic stocks (Fig. 14). The dike was sampled for Ar-Ar geochronology and yielded an age of 13.4 Ma (sample P-20 in Table 1; Fig. 4N).

PALINSPASTIC RECONSTRUCTION OF CENOZOIC DEFORMATIONS

A rigorous palinspastic reconstruction should restore geologic features created just prior to the deformation being reconstructed to eliminate the effects of other older deformation events. If such features do not exist, then the next best scenario is to restore features created during the early period of deformation to obtain a minimum displacement. The Miocene volcanic-sedimentary sequence and related intrusion zones described

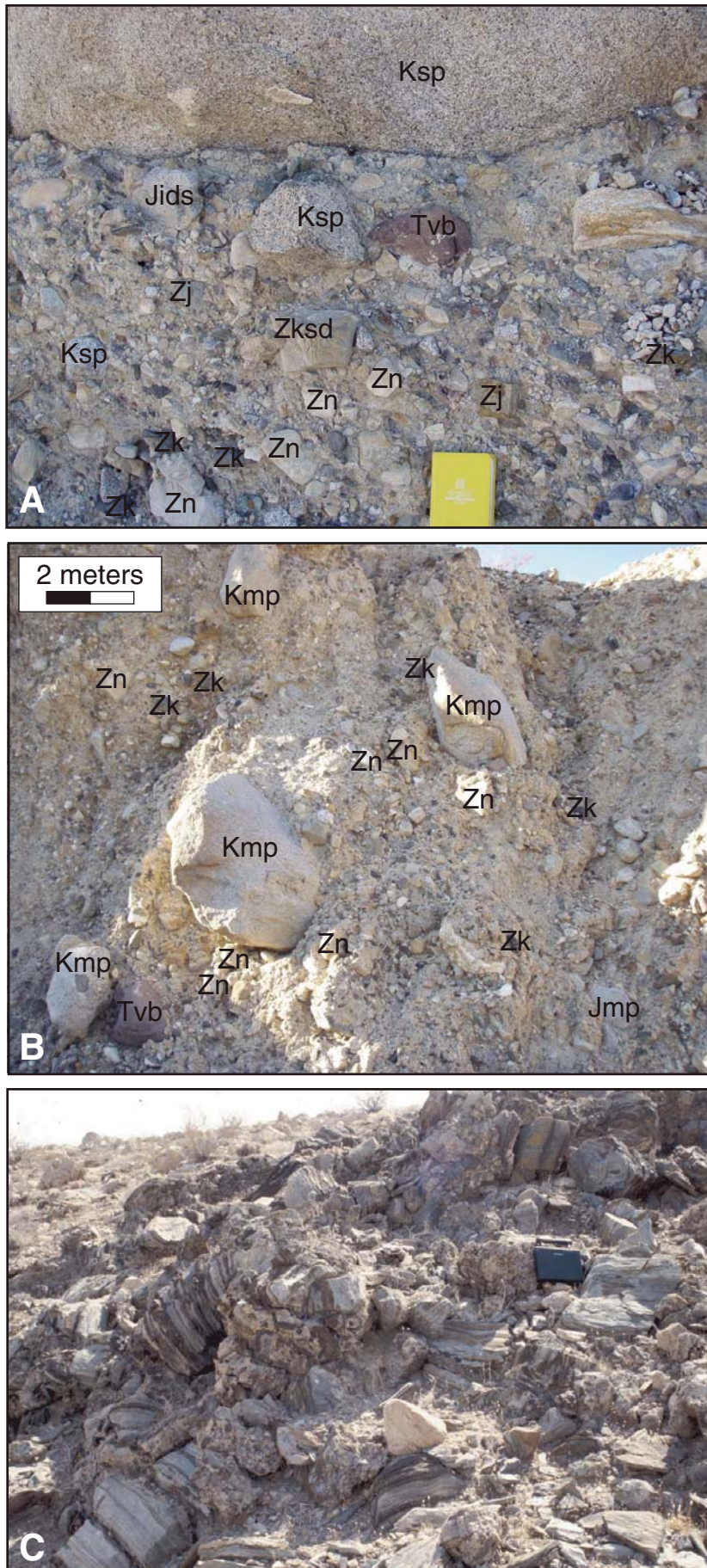


Figure 8. Photographs of Panamint Valley inselberg sediments. (A) Northern facies of massive conglomerate. Field notebook (12 x 19 cm) for scale. (B) Southern facies of massive conglomerate. (C) Monolithologic breccia deposit in the northernmost exposures of the inselbergs. The clast rock type present in this photograph is greenish-gray, laminated calc-silicates that are correlated to the lower portions of the Neoproterozoic Johnnie Formation, as exposed in the southern Panamint Range. The laptop computer is 25 cm wide. Several clast rock types are denoted on these photographs; these are briefly described and their interpreted source rock unit is given in parentheses: Ksp—Cretaceous South Park granodiorite; Kmp—Cretaceous Manly Peak quartz monzonite; Jids—Late Jurassic Independence Dike Swarm; Tv—Miocene or older volcanic lava flows; Zj—Neoproterozoic Johnnie Formation; Zn—Neoproterozoic Noonday Dolomite; Zk—Neoproterozoic South Park Member of the Kingston Peak Formation; and Zksd—Neoproterozoic Sourdough Limestone Member of the Kingston Peak Formation.

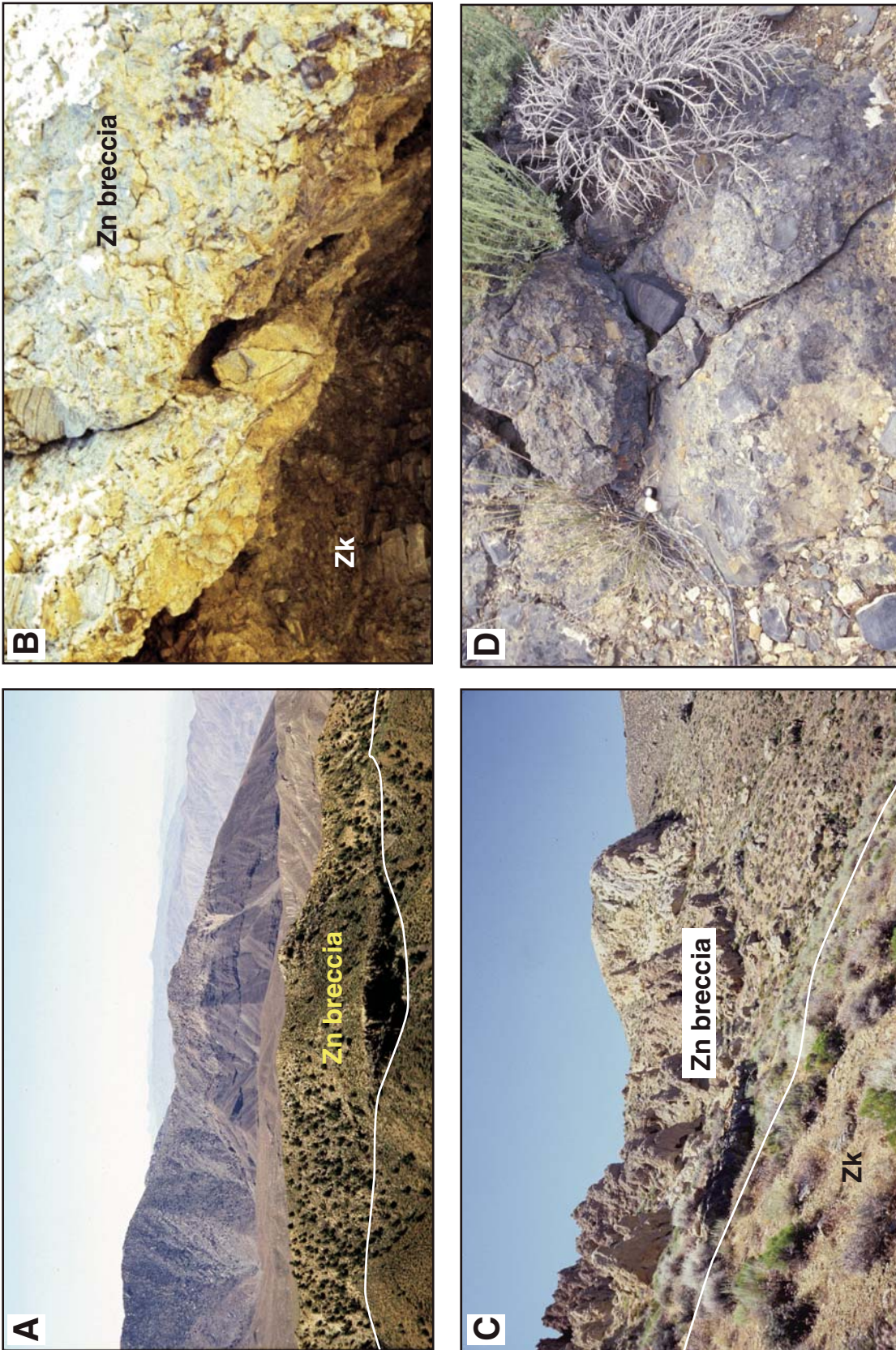


Figure 9. Photographs of monolithic breccia deposits along the western flank of the central Panamint Range. (A) Breccia deposit along the south side ridge of South Park Canyon, looking to the south. Breccia of yellow metadolomite (labeled Zn breccia) is correlated to nearby exposures of Noonday Dolomite. This breccia deposit overlies in-place Kingstons Peak Formation with intervening upper member of the Kingstons Peak Formation (Pleasant Canyon Member) missing along the contact. Piñon trees are 2–3 m tall. (B) Detailed photograph of the base of one of the monolithic breccia deposits of Noonday Dolomite over strongly fractured but in-place Kingstons Peak Formation rocks (labeled Zk). This view is 1 m across. (C) Intermediate scale view of the breccia deposits of Noonday Dolomite over in-place Kingstons Peak Formation. Note the distinct packages or lenses of clast lithologies that compose the breccia deposit, shown here by variations in color and texture. Scale varies in this view; the bushes are ~1 m tall. (D) Detailed view of monolithic breccia of Sourdough Limestone Member of the Kingstons Peak Formation showing angular clasts bound in fine matrix without apparent pore space. Note hand lens for scale.

Reconstructing late Cenozoic deformation in central Panamint Valley

above are such features formed during the early period of deformation; we use them to reconstruct the net 0–15 Ma ago deformation across Panamint Valley.

Reconstruction of Inselberg Sedimentary Sources

A robust reconstruction marker exists in the basal portion of the Miocene succession at the inselbergs near Highway 178 in western Panamint Valley (Figs. 3A and 7). The clast assemblage closely matches the rock types and metamorphic grades of pre-Cenozoic intrusive and metamorphic rocks in the southwestern Panamint Range (Johnson, 1957; Albee et al., 1981; Cichanski, 1995; Andrew, 2002). This is the only area where an appropriate suite of source rocks is exposed. In addition, the spatial distribution of rock types as clasts in the conglomerates at the Panamint Valley inselbergs matches the bedrock exposures in the southern Panamint Range. To the south of Redlands Canyon, the most common rocks high in the Range are Kingston Peak Formation and Manly Peak quartz monzonite (coarse grained, and biotite and hornblende bearing with very light pink porphyritic potassium feldspar; Johnson, 1957; Cichanski, 1995; Andrew, 2002). These are the common clast type in the southern inselberg exposures (A in Figs. 7 and 16). Northward, the axial portion of the Panamint Range is dominated by exposures of Neoproterozoic rocks as well as the South Park Canyon granodiorite (coarse grained, porphyritic, and biotite bearing with locally strong S-C fabrics, augen, and crosscutting mylonite shear zones). A clast assemblage of these rock types is common in the inselberg exposures just north of Highway 178 (B in Figs. 7 and 16). North of South Park Canyon, the upper portions of the Panamint Range are mantled by Noonday Dolomite and Johnnie Formation, both in place and in breccia sheets. These two rock units dominate the clast types present in the conglomerates at the northern inselbergs (C and D in Figs. 7 and 16).

The western flank of the Panamint Range below elevations of 1200 m (900 m above the valley floor) has several rock units that are absent as clasts at the inselbergs. Coarse-grained hornblende diorite dominates the exposed range face to the south of Redlands Canyon (Fig. 16). The lower exposures along the Panamint Range front from Redlands Canyon northward (Fig. 16) to Happy Canyon are quartz-feldspar gneiss and metadiabase. Only two clasts of quartz feldspar gneiss have been found at the inselbergs, and these occur within the upper beds of the southeasternmost expo-

ures of this unit. Two Cretaceous granitoids are also exposed along the western Panamint Range below 1200 m elevation: a deformed granodiorite with ubiquitous, strong mylonitic textures (mylonitic granodiorite of Pleasant Canyon of Andrew, 2002) that occurs several kilometers north of Redlands Canyon between Middle Park

and Happy Canyons (Fig. 3B); and a coarse-grained, garnet-bearing, light-colored alkali-feldspar granite (granite of Redlands Canyon of Andrew, 2002) that only crops out in lower Redlands Canyon below 1100 m elevation (Fig. 16). Neither of these two plutonic rocks has been found in the inselberg Miocene conglomerates.

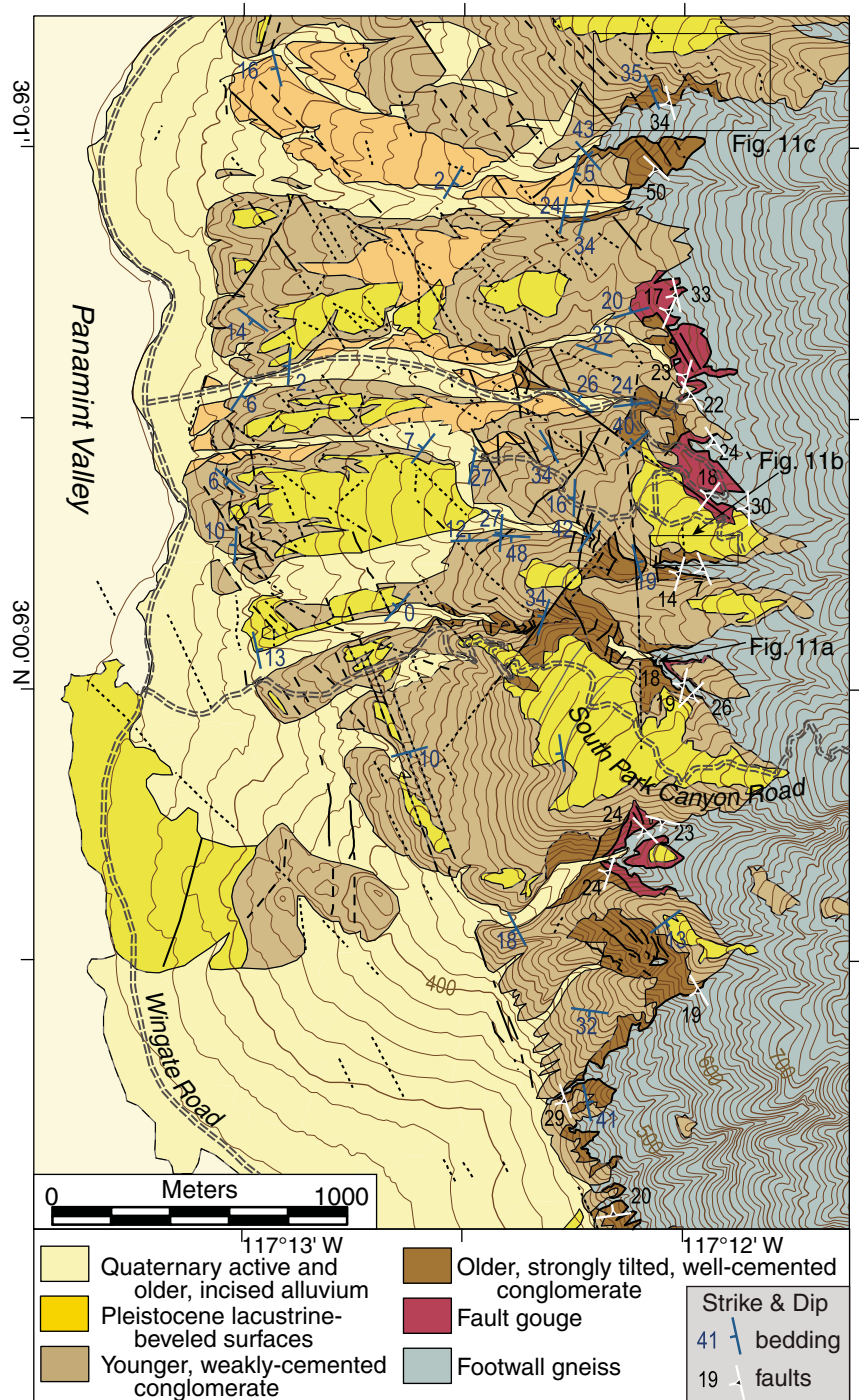


Figure 10. Detailed geologic map of Miocene(?) and younger units along a portion of the range front of the Panamint Range near South Park Canyon. The number of faults and structural data has been greatly simplified for this scale.

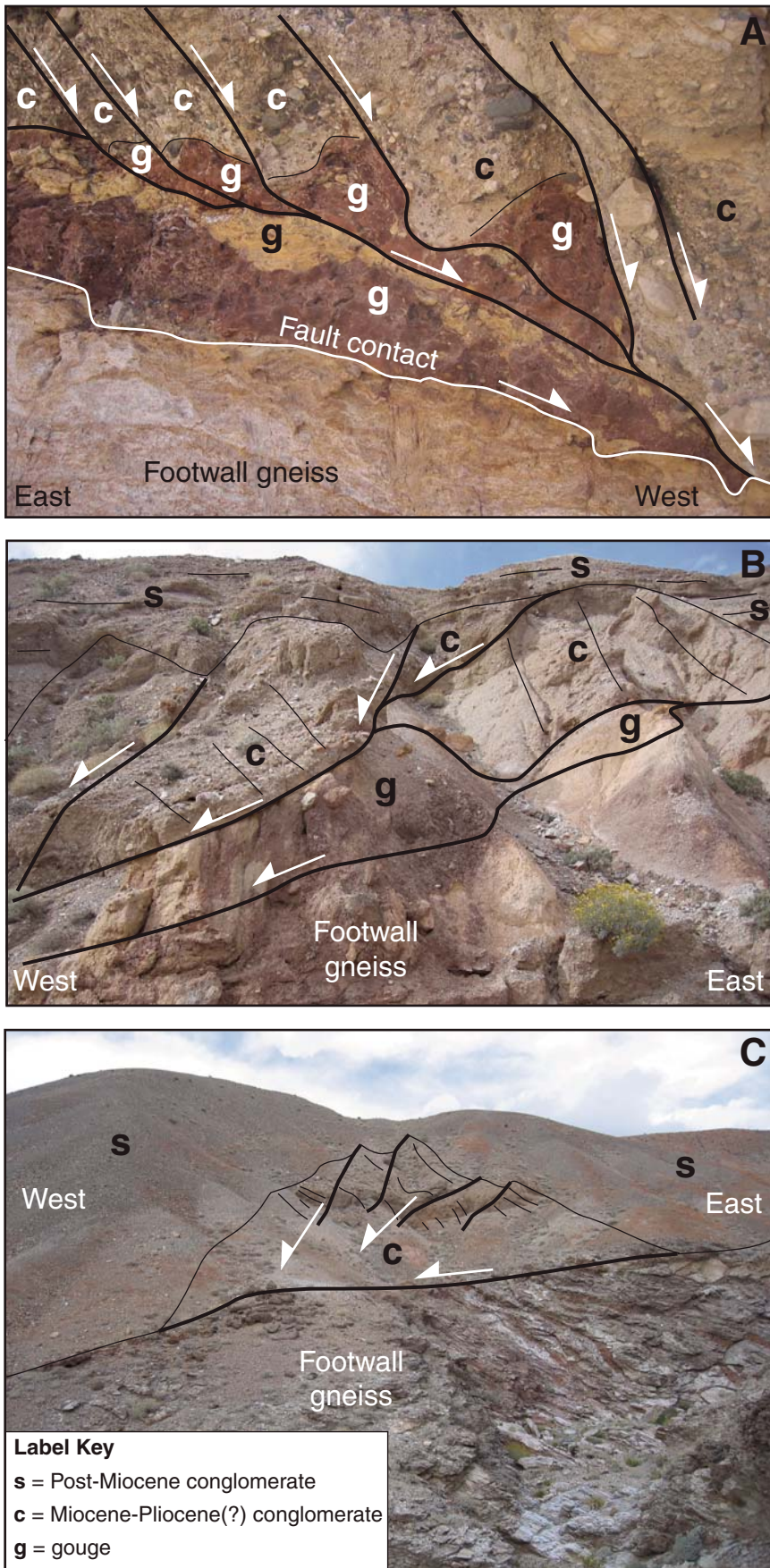


Figure 11. Photographs of relationships between younger and older strata along the front of the Panamint Range shown in Figure 10. (A) Footwall gneiss in fault contact with fault gouge derived from the gneiss, with hanging wall of older Miocene or Pliocene conglomerates that have a foot-wall sedimentary source. The hanging-wall conglomerate is strongly faulted and back-tilted. View is approximately 2 m wide. (B) Relationships of footwall gneiss, fault gouge, and deformed older set of conglomerates, which are overlain by a younger set of conglomerates. This younger conglomerate is not faulted, tilted, or in fault contact with the other units. The yellow bush in the foreground is 75 cm tall, and the hillside is approximately 9 m tall. (C) Set of older conglomerates in fault contact with the detachment fault and unconformably overlain by younger conglomerates deposited onto the fault surface. Note the differential erosion between the two conglomeratic units: this is due to the strong cementation of the older units compared to the younger unit. The yellow bush in the foreground is 75 cm tall, and the steep hillside is approximately 35 m tall.

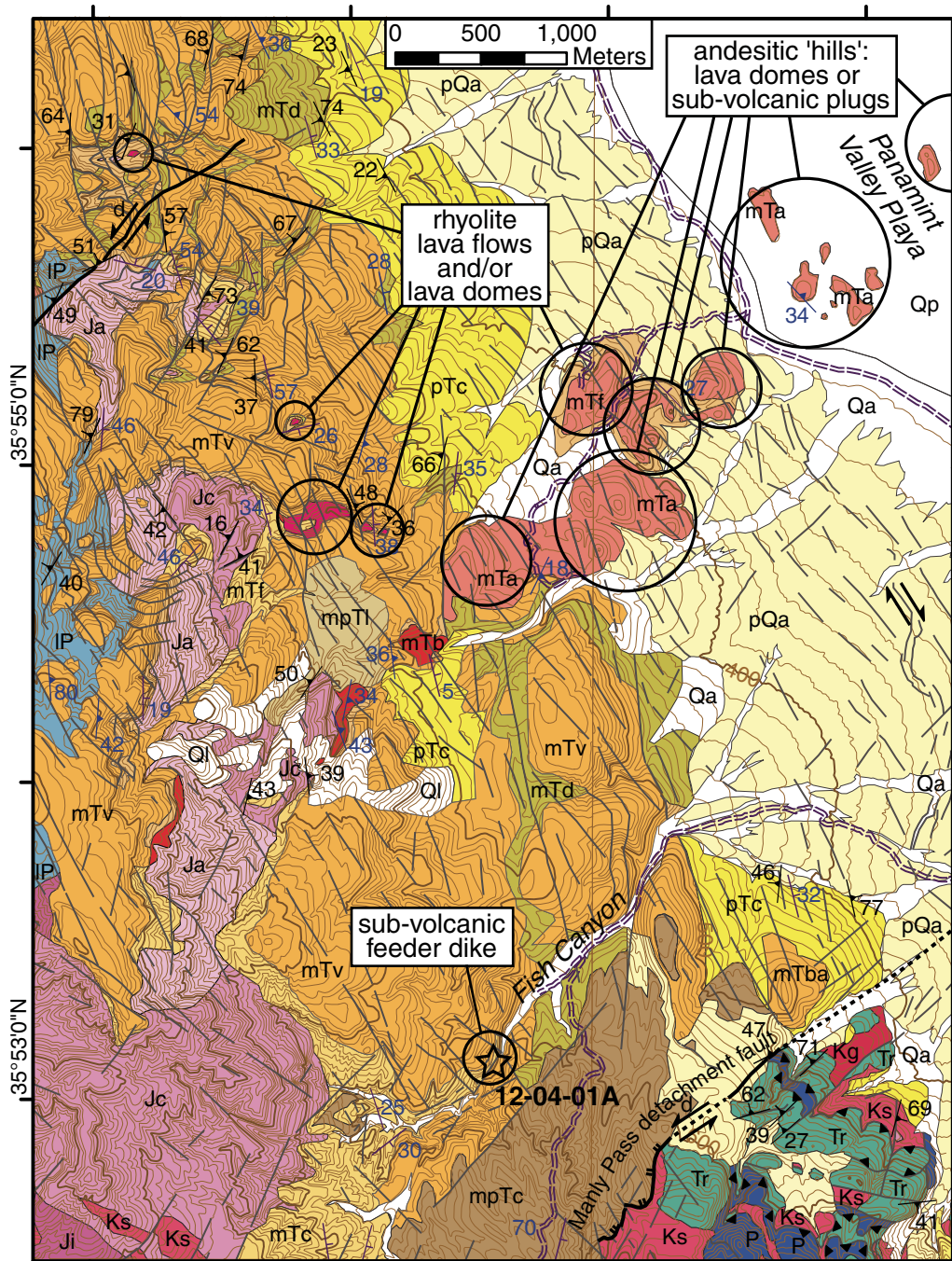
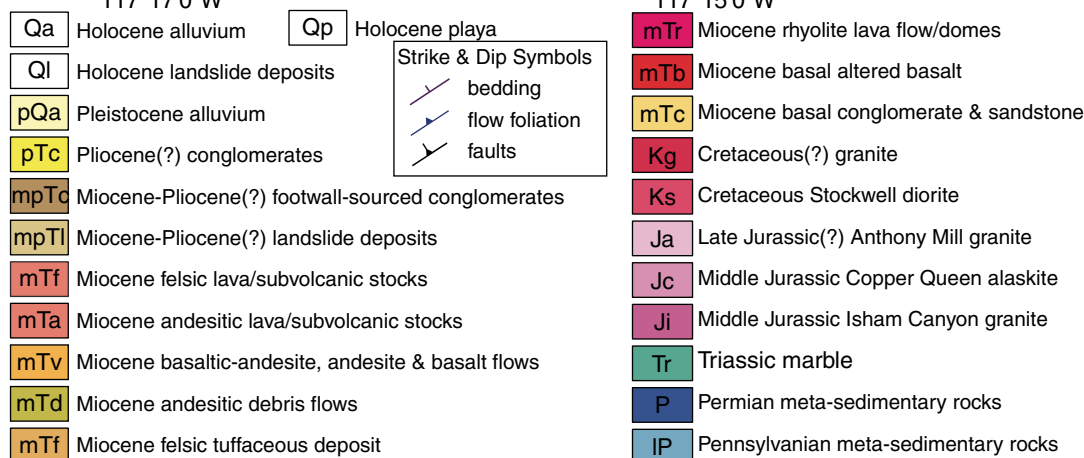


Figure 12. Simplified geologic map of the Fish Canyon area of the Slate Range (see Fig. 3A for location). Faults are shown by thick lines; the two darker lines are larger displacement faults mentioned in the text. All of the faults shown are Cenozoic, except the thrust faults in the lower right corner. Sense of shear is shown for several faults using sets of arrows, with a d symbol on the down side of normal faults, or with hanging-wall side teeth for Mesozoic thrust faults. Miocene intrusive or near-vent facies units are circled for clarity.



A reconstruction vector for the Miocene conglomerates at the inselbergs can be interpreted from these observations. The coarse clast size of the conglomerate suggests that they were close to their source area at time of deposition. Clasts with sizes similar to those found in the inselberg conglomerates are only found in the

modern fans along the Panamint Range within ~2 km of the range front. The rock units present as clasts in the inselberg conglomerates point to a source near present-day Redlands Canyon. Redlands Canyon is the only location where all of the matching metasedimentary and intrusive units coincide (units Ks, Km, Zj, Zn, and Zk in

Fig. 16). The rock units exposed along the lower elevations of the western flank of the Panamint Range that are not represented in the inselberg conglomerates (units Kr, Jh, and Y in Fig. 16) might not yet have been exhumed by normal faulting during the time of Miocene conglomerate deposition. The source for all of the inselberg units, including the monolithologic breccia masses, is now at an elevation >1200–1400 m. The source area for the inselberg conglomerates must have been relatively near the western Panamint Range, because a source too far to the east would not have sampled the South Park Canyon granodiorite body (unit Ks in Fig. 16). The South Park Canyon granodiorite occurs as a steep-sided, narrow (<1 km wide) intrusion along the upper portion of the range front.

If we reconstruct the inselberg rocks to near the middle elevations of the western Panamint Range flank at Redlands Canyon, placing each major clast assemblage to within ~2 km of a similar source, we derive a displacement of ~17 km of motion toward ~300°. This model fits all of the clast composition constraints except one, the blue recrystallized limestone. The only exposed source of this rock in the southern Panamint Range is weakly metamorphosed, blue, Pennsylvanian–Permian Bird Spring Formation limestones at Striped Butte in Butte Valley (unit PP in Fig. 16; Johnson, 1957; Stone, 1985; Wrucke et al., 1995). Redlands Canyon currently ends eastward at a wind gap with Butte Valley (Fig. 16). Removing 20°–30° of eastward tilting of the Panamint Range (Maxson, 1950; Johnson, 1957; McKenna and Hodges, 1990; Cichanski, 1995) would place Butte Valley at the headwaters of a paleo-Redlands Canyon, which would provide a drainage route for clasts from Striped Butte to be transported toward the inselberg sediment source area.

The discussion above assumes that the coarse sedimentary rocks were deposited during early normal faulting along the western Panamint Range. This would create the necessary exposures and topographic relief to mobilize and transport these clasts, and account for the generally eastward thickening exhibited by the Miocene sedimentary and volcanic sequence. Faulting of this age and character is documented in the Panamint Valley area (e.g., Hodges et al., 1990; Snyder and Hodges, 2000; Walker et al., 2005). In addition, we assume that the deposition center corresponds closely to the current range-bounding fault of the Panamint Range. This is probably a reasonable assumption in that there are no preserved large-magnitude normal faults in Panamint Valley west of the Panamint Range front and there are no exposures of the distinctive rocks or metamorphic grades of the Panamint Range west of Panamint Valley. The

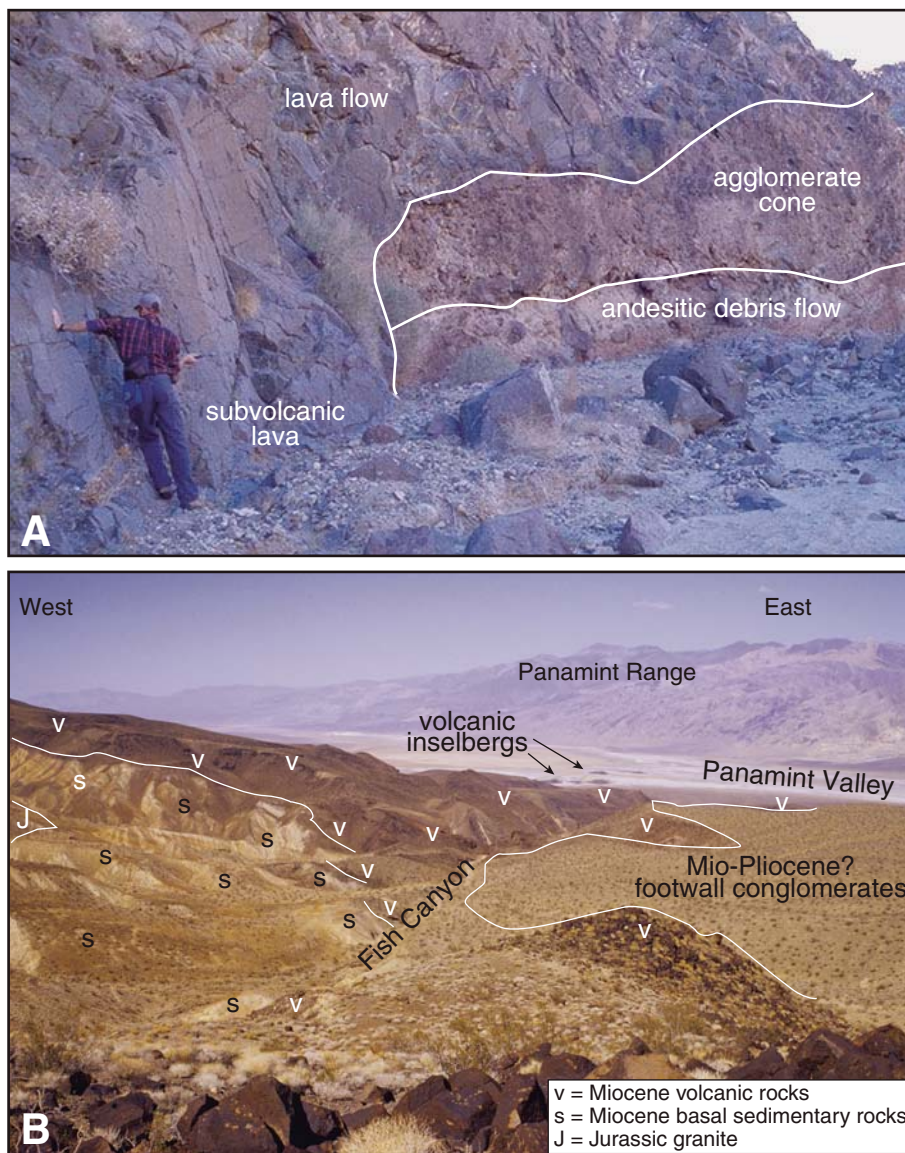


Figure 13. Photographs from the Fish Canyon area of the Miocene volcanic-sedimentary succession in the Slate Range. (A) Outcrop in Fish Canyon of an agglomerate cone on top of a monolithologic, andesitic debris-flow deposit intruded by basaltic magma, which then grades into a lava flow that covers and flows beyond the cone. The basaltic intrusion trends northeastward. Geologist for scale. (B) View of Fish Canyon from Manly Pass showing the basal nonconformity with Jurassic granite, overlain by conglomerate and then capped by voluminous basaltic-andesite lavas. This image also shows the andesitic and rhyolitic composition inselbergs within the playa of Panamint Valley. The thickness of the Miocene units is difficult to estimate based on the presence of numerous faults, but it is at least 200 m. The Panamint detachment can be seen in the background where Panamint Valley meets the Panamint Range.

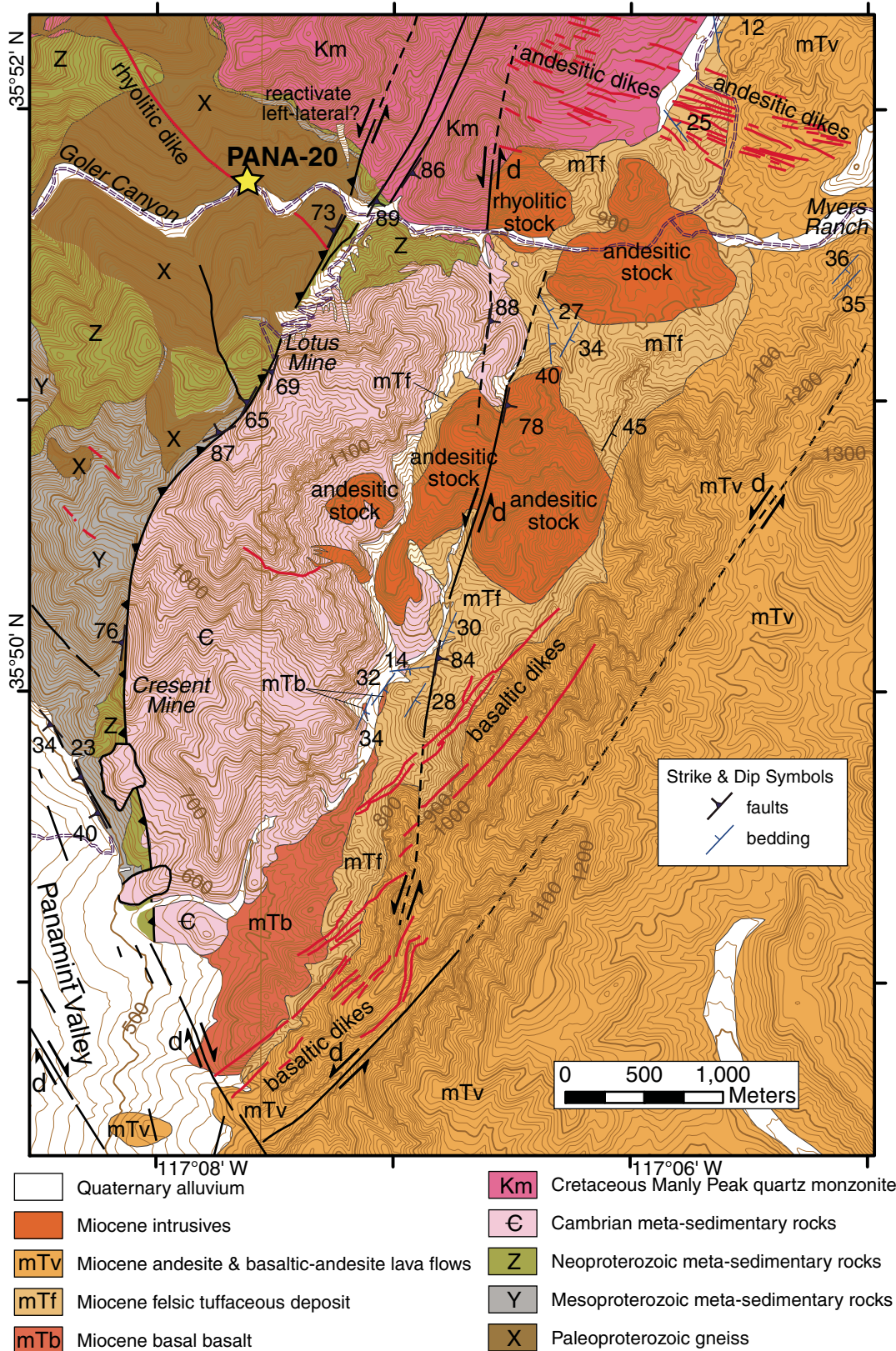


Figure 14. Simplified geologic map of the Goler Canyon area of the southern Panamint Range (see Fig. 3A for location). All of the faults are Cenozoic, except the thrust fault, which is Mesozoic but has some Cenozoic reactivation. Note that the thrust fault is Mesozoic. The yellow star denotes the location of a geochronology sample.

uncertainties of this reconstruction marker are ~2 km, similar to the observed limit of coarse (>2 m diameter) clasts transported by debris-flow processes along the active flank of the Panamint Range.

Reconstruction of Miocene Intrusive and Near-Vent Rocks

Another displacement vector can be derived from Miocene near-vent and intrusive igneous rocks in the Slate and Panamint Ranges. There is a strikingly similar set of dikes and intrusives in Goler Canyon area of the southwestern Panamint Range and in the Fish Canyon area of the northern Slate Range (Fig. 17A). There are four intrusive zones in the Goler Canyon area: (1) a linear arrangement of northeast-trending stock-like andesitic intrusives that start in Goler Canyon and continue northeastward for 6 km; (2) a rhyolitic stock in Goler Canyon; (3) a series of southwest-striking mafic dikes that begins south of Goler Canyon; and (4) a northwestward-striking rhyolitic dike in Goler Canyon (Figs. 14 and 17A). The Fish Canyon area has a similar set of features with similar geometry: (1) a linear arrangement of deeply weathered andesitic hills trending to the north-northeast; (2) one of the deeply weathered hills near the southwest end of the linear trends has a lighter color index and thus could be more rhyolitic in composition; (3) a northeast-striking basaltic dike intruding an agglomerate volcanic cone

exposed in central Fish Canyon (Figs. 12 and 13A); and (4) a north-northwest-trending series of exposures of rhyolitic domes (Figs. 12 and 17A). The distinct geometry of these intrusive zones can be used to create a piercing line to match the Fish Canyon area with Goler Canyon. Figure 17B shows the restoration of the Fish Canyon intrusives and near-vent facies volcanics over the intrusive zones in the Goler Canyon area across Panamint Valley. This places the late-stage possible andesitic domes or near-surface plugs of the northern Slate Range on top of the andesitic stocks in the southern Panamint Range. This also aligns the basaltic feeder dike and vent complex of Fish Canyon with the basaltic dikes south of Goler Canyon, and places the late-stage, lighter color-index dome or plug over the rhyolitic stock in Goler Canyon. The reconstruction assumes that the Slate Range rocks are in the hanging wall and Panamint rocks in the footwall of the proto- and/or current Panamint bounding fault.

The intrusives at Fish Canyon are calculated to have been displaced 14.7 km along an azimuth of 296° (shown in Fig. 17B). This is a maximum estimate of ~14 Ma old displacement, because any larger amount would place the Fish Canyon rocks on top of coeval volcanic strata of the southern Panamint Range, a clearly unacceptable condition. The ~2.5 km shorter difference of this vector relative to the one derived from the

inselberg sediment source is due to faulting in the northern Slate Range between Fish Canyon and the inselberg conglomerate outcrops. Two major southwest-striking faults occur in the northern Slate Range (both shown in Fig. 17B) that have left-lateral oblique normal slip, similar to the Manly Pass fault (Walker et al., 2005; Numelin et al., 2007a), which could accommodate the few kilometers of north-northwest-directed displacement, accounting for the offset difference.

Southern Slate Range

Reconstructing the Miocene position of the southern Slate Range relative to the Panamint Range is more problematic. No Miocene volcanic or sedimentary rocks occur in the studied portion of the southern Slate Range, although such deposits are on the east side of this range ~15 km to the south. The pre-Cenozoic rocks of the southern Slate Range do not obviously match rocks in the Panamint Range or Owlhead Mountains, but they do match rocks in the northern Slate Range. Thus the southern Slate Range can be restored to the Panamint Range by its displacement relationships with the northern Slate Range. The displacement between these two parts of the Slate Range is determined by aligning the contact point of three rock units: a Jurassic granite, a Cretaceous diorite, and deformed late Paleozoic-early Mesozoic metasediments. This contact occurs at the northeasternmost corner of the southern Slate Range, and matches a

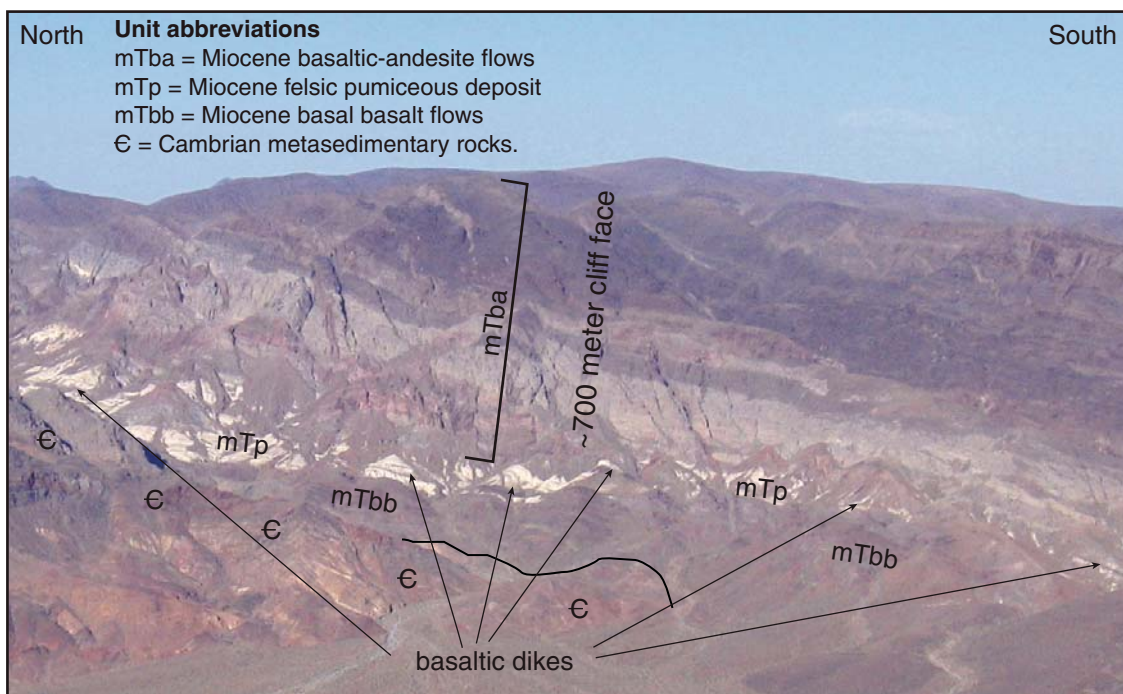
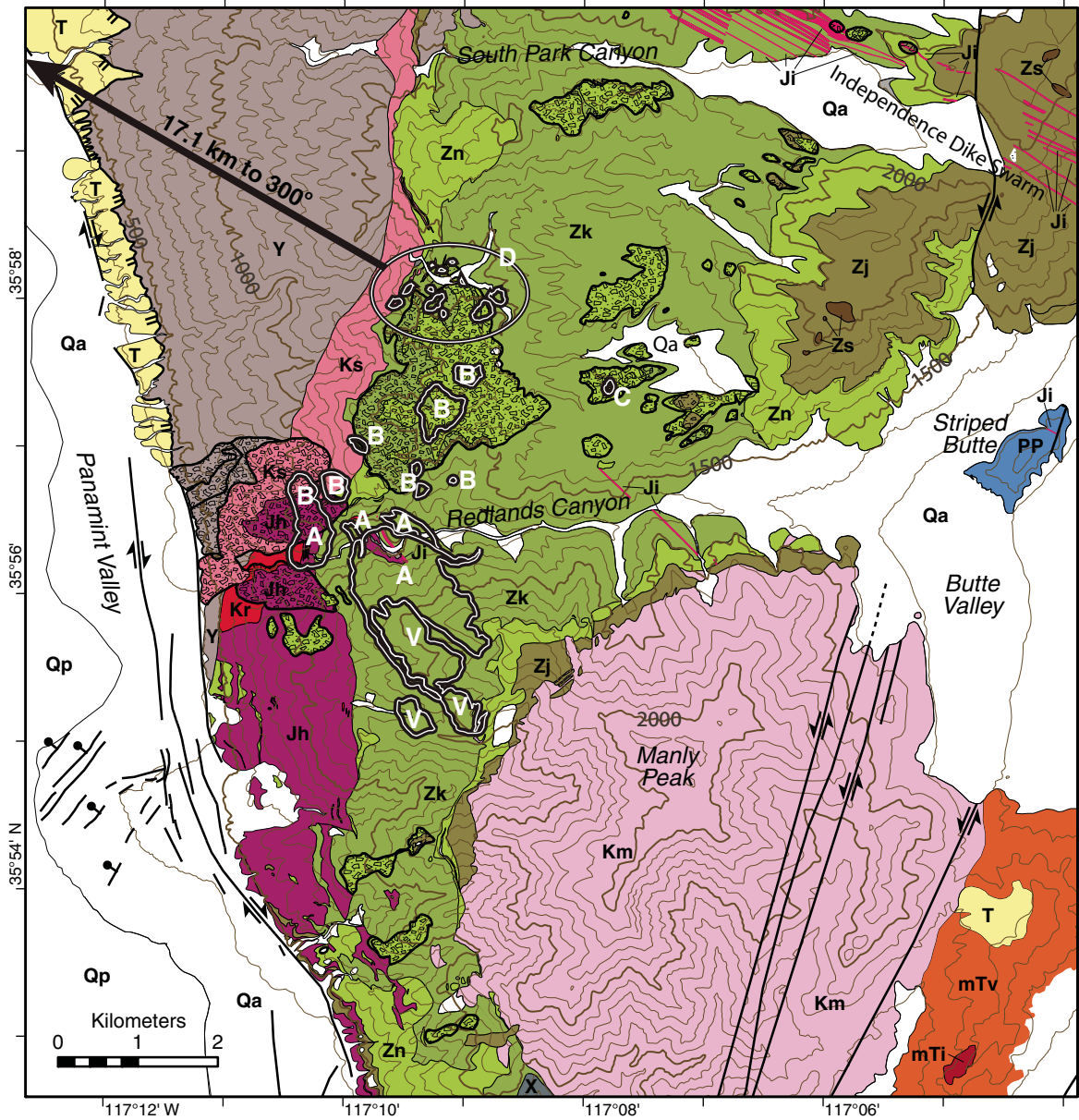


Figure 15. Photographs of nearly complete exposures of the Cenozoic volcanics in the southwestern Panamint Range.



Geologic Units

Tertiary

- Qp - Holocene playa
- Qa - Holocene alluvium
- T - Miocene(?) - Pliocene fanglomerates
- mTx - Miocene monolithologic breccias
Pattern background color/texture indicates source rock unit of each breccia.
- mTv - Miocene volcanics
- mTi - Miocene subvolcanic intrusions

Cretaceous

- Kr - Granite of Redlands Canyon
- Ks - South Park Granodiorite
- Km - Manly Peak Quartz Monzonite

Jurassic

- Ji - Independence Dike Swarm
- Jh - Hornblende Diorite

Pennsylvanian-Permian

- PP - Bird Spring Formation

Neoproterozoic

- Zs - Stirling Quartzite
- Zj - Johnnie Formation
- Zn - Noonday Dolomite
- Zk - Kingston Peak Formation

Mesoproterozoic

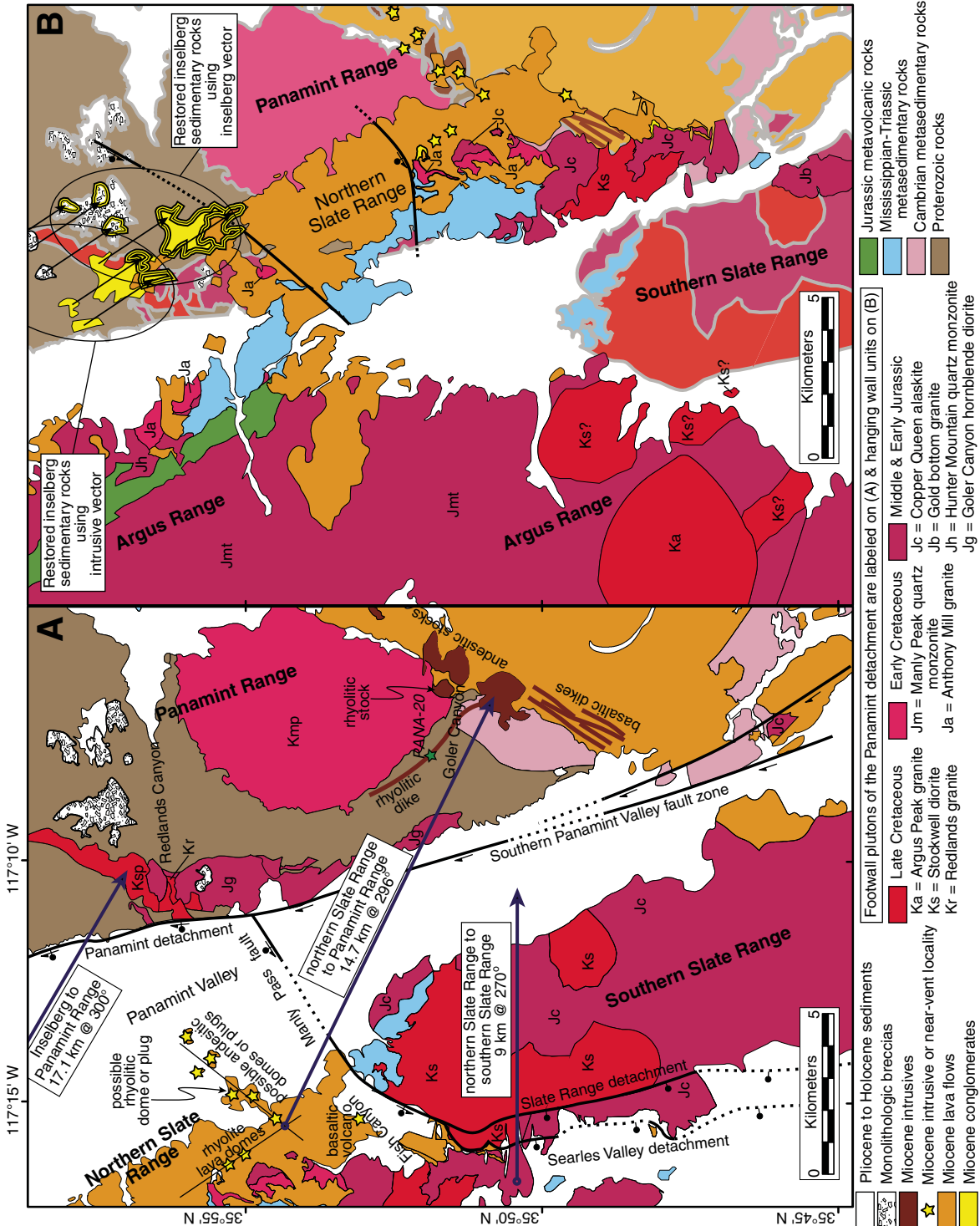
- Y - Crystal Spring Formation

Paleoproterozoic

- X - orthogneiss

Figure 16. Simplified geologic map of the Redlands Canyon region of the Panamint Range. Placed over this is the restored outline of Panamint Valley inselberg deposits, shown by white lines outlined in black. The displacement vector is the labeled large arrow. The different units in the inselberg deposits are labeled in white text, using the same key as in Figure 7, except V, which is volcanic rocks. The placement of the boundary between the northern and southern facies of the inselberg conglomerates straddles Redlands Canyon for north-south placement control and near the outcrop of the north-south-trending South Park Canyon granodiorite (labeled Ks), which is one of the significant sources for conglomerate B at the inselbergs. Note the wind gap between Redlands Canyon and Butte Valley; clasts from Striped Butte in Butte Valley may have traveled down paleo-Redlands Canyon to contribute to the inselberg sediments. See text for further discussion of the source area for Panamint Valley inselberg basal conglomerates. Modified from Johnson (1957), Smith (1979), Cichanski (1995), and Andrew (2002).

Figure 17. Palinspastic reconstruction constraints for southern Panamint Valley based on restoring Miocene intrusives and near-vent facies in the northern Slate Range and the southern Panamint Range. (A) Simplified geologic map of the current geology showing our interpreted reconstruction vectors (thick blue lines) to restore selected geologic features. (1) The northern Slate Range relative to the Panamint Range is determined by combining the intrusive zones of these two areas with the northern Slate Range in the hanging wall. (2) The northern to the southern Slate Range is determined by reconstructing the intrusive contacts of a Cretaceous pluton that intruded a Jurassic pluton contact with late Paleozoic-Triassic metasedimentary rocks, and by a thermochronologic datum determined by Didericksen (2005). Modified from Walker et al. (2002, 2005). (B) Reconstruction based on the two vectors shown in A. The northern Slate Range units are outlined in black lines, while the rocks of the underlying footwall rocks of the southern Slate Range and Panamint Range are shown with wide light gray outlines. Two major left-lateral, oblique normal faults are shown in the northern Slate Range that have displacement amounts and orientations that could account for the mismatch between the two reconstruction vectors for the inselberg Miocene sedimentary rocks.



similar zone in the southwesternmost portion of the northern Slate Range that is interpolated to be under alluvium in Searles Valley (Fig. 17B), giving an ~8–10 km westward displacement of the northern Slate Range relative to the southern Slate Range. This displacement must have occurred by slip on the Slate Range detachment and Searles Valley–Manly Pass fault zones. This vector is similar to the 9 km to 270° horizontal vector (Fig. 17A) determined from thermochronology data of the southern Slate Range by Didericksen (2005). The displacement of the southern Slate Range relative to the Panamint Range can then be calculated by subtracting the northern Slate Range–southern Slate Range vector from the northern Slate Range–Panamint Range vector. The calculated displacement vector for the southern Slate Range relative to the Panamint Range is 10.5 km to 325°.

Interpretations and Implications for Previous Models and Regional Structural Development

The reconstruction presented here (Fig. 18) differs significantly from previous studies (Figs. 2B, 2C, 2D). Our reconstruction vector for the Argus Range is ~17 km displacement from the Panamint Range, whereas previous reconstructions had 53–23 km of displacement. The azimuths of the Argus Range displacement are similar between our model and the interpretations of Snow and Wernicke (2000) and McQuarrie and Wernicke (2005), but the vector of Serpa and Pavlis (1996) is slightly more northward. Our displacement vector to move the southern Slate Range away from the Panamint Range is distinctly different from those of previous studies. The displacement vectors of Snow and Wernicke (2000) and McQuarrie and Wernicke (2005) are much longer, but the azimuth of the Snow and Wernicke (2000) vector is the same as our newly determined vector. The vector of Serpa and Pavlis (1996) is somewhat anomalous, but the overall position of the Slate Range relative to the Panamint Range is similar to our findings. Two of the previous studies had significant vertical axis rotation of the range blocks. We assume no differential vertical axis rotations in our reconstructions based on observations of the numerous Independence Dike Swarm dikes in the Argus, Slate, and Panamint Ranges, all of which have similar strikes (Moore, 1976; Andrew, 2002).

There are two explanations for the discrepancies of our displacement vectors from those previously published: (1) incomplete and incorrect correlation of structural markers and magnitudes of fault offsets, and/or (2) pre–15 Ma ago to post-Late Cretaceous deformation event(s)

that accommodate a significant amount of displacement (e.g., Hodges and Walker, 1990; Applegate et al., 1992). We explore the latter possibility in the following.

The reconstruction criteria used for our displacement vectors are completely different from those of the previous studies. The displacement vector for the Argus Range from the Panamint Range by McQuarrie and Wernicke (2005) was a result of adding two displacement vectors: (1) the $\sim 9 \pm 1$ km to azimuth 305° reconstruction of 4.2 Ma old basalts along the Hunter Mountain fault (Burchfiel et al., 1987; Sternlof, 1988), and (2) the 22 ± 3 km to azimuth 315° reconstruction of a Cretaceous backfold (Wernicke et al., 1988; Snow and Wernicke, 1989, 2000; Snow and Wernicke, 2000; Lux, 1999). Similarly, Serpa and Pavlis (1996) used these two offset constraints along with observations of structures in the southern Panamint and Death

Valley areas. The reconstruction of Snow and Wernicke (2000) was based on the fit of regional late Paleozoic and Mesozoic thrusts, but the Panamint Valley portion of their reconstruction also included deformation accommodated by the Tucki Mountain detachment system, which was a reconstruction of the Cretaceous backfold. The regional Cenozoic reconstructions of Snow and Wernicke (1989) and McQuarrie and Wernicke (2005) of 250–300 km of displacement across the central Basin and Range would not be greatly affected by this new Panamint Valley data, since their reconstruction transects are north of Panamint Valley and do not involve the Argus Range.

Harrisburg Fault of the Tucki Mountain Detachment System

All three previously published displacements for the Panamint valley area used reconstruction

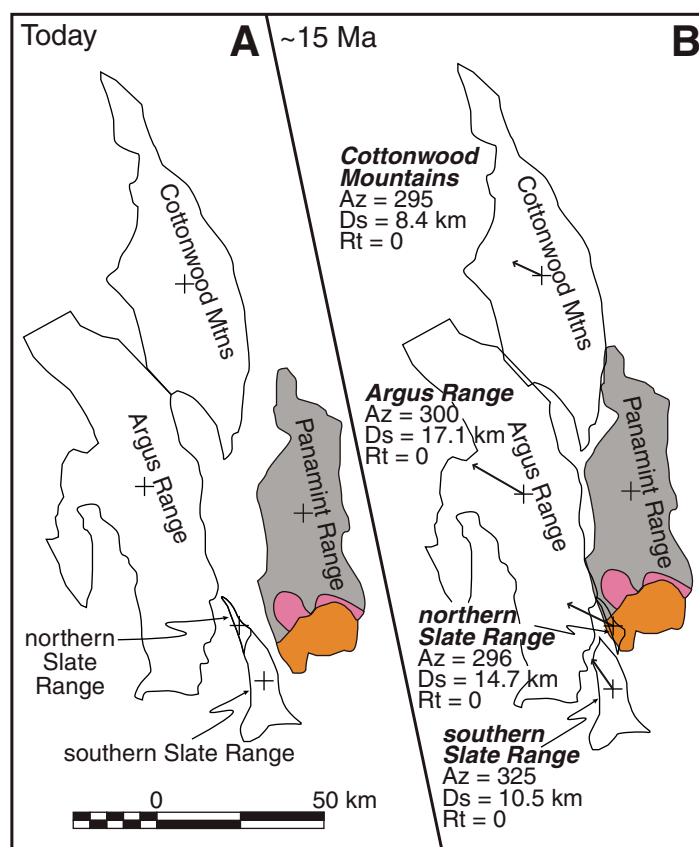
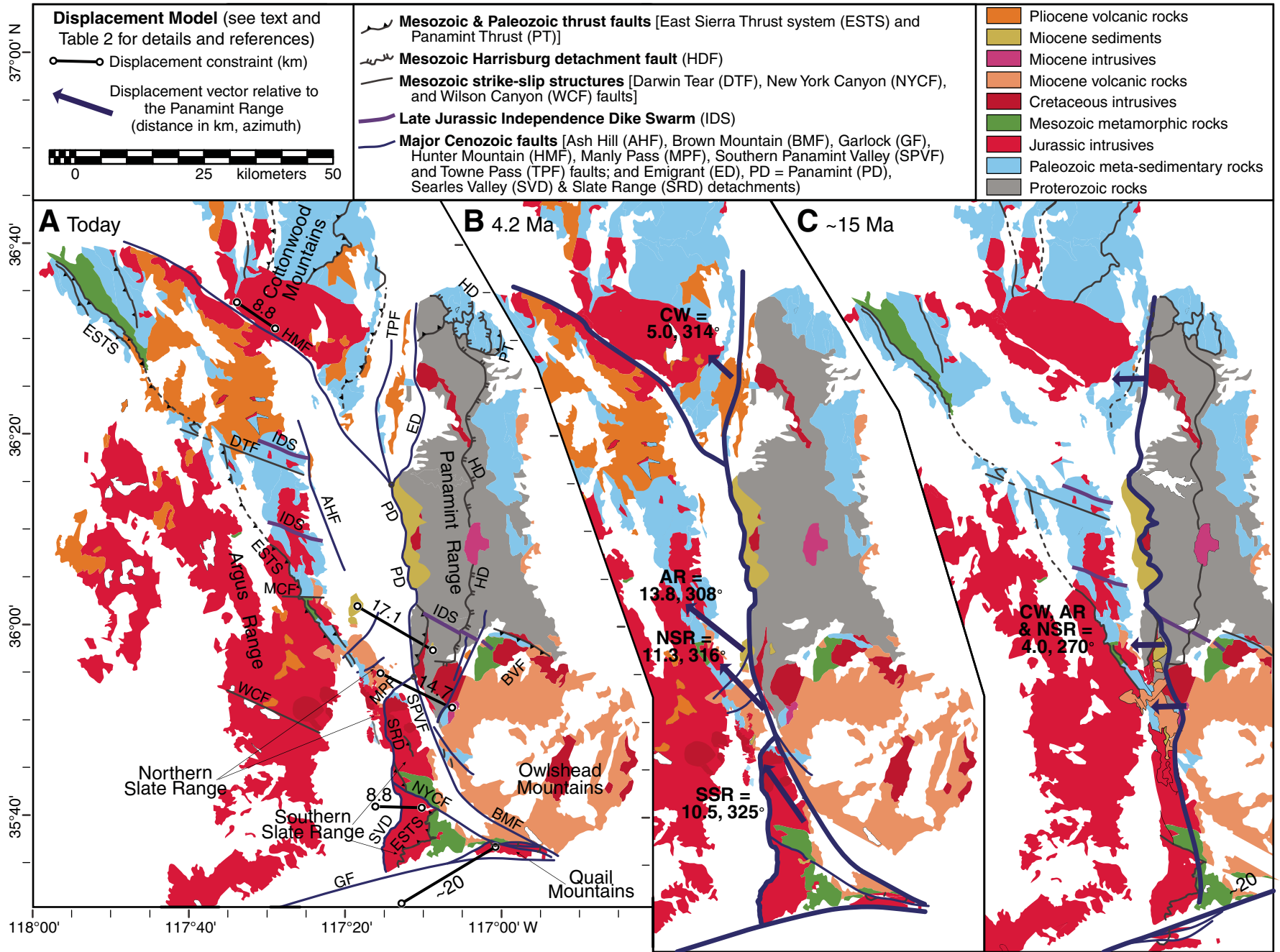


Figure 18. Our new palinspastic reconstruction displacement vectors relative to the Panamint Range for the Panamint Valley region. (A) Current configuration of the ranges surrounding Panamint Valley. See Figure 2 for symbol key. (B) Restored range blocks ca. 15 Ma ago using our new displacement vectors for the Argus and southern Slate Ranges. The Cottonwood Mountains are restored using the new Argus Range vector combined with the Hunter Mountain fault displacement vector of Burchfiel et al. (1987). Compare this reconstruction with published reconstructions shown in Figures 2B–2D.



of a Cretaceous age backfold as a key constraint. The offset of this backfold is attributed to the Tucki Mountain detachment system (Wernicke et al., 1988; Snow and Wernicke, 1989), which includes the Emigrant fault and the Harrisburg fault subsystems. The Emigrant fault portion has the youngest provable deformation. The older portion of Tucki Mountain detachment system is the Harrisburg detachment. The displacement data for the Tucki Mountain detachment system do not specify which of these faults accommodated the strain.

The Harrisburg detachment is significantly different from the other structures in the Panamint Valley region. This fault system is strongly backtilted eastward and is domed over the northern Panamint Range (Fig. 19A) (Wernicke et al., 1986; Hodges et al., 1989, 1990). Other Cenozoic normal extensional faults of the Panamint Valley area are backtilted to a lesser degree or not at all (Cichanski, 2000; Walker et al., 2005; Didericksen, 2005; Numelin et al., 2007a). In addition, the footwall to the Harris-

burg detachment has associated ductile folds and north-northwest-trending ductile stretching lineations (Wernicke et al., 1986, 1988; Hodges et al., 1987, 1990), whereas other late Cenozoic faults in the Panamint Valley area do not have known associated ductile deformation. The age brackets on the deformation of the Harrisburg detachment are between ca. 100 and 11 Ma ago (Hodges et al., 1990). Thus, a portion of the deformation of the Tucki Mountain detachment must be older than ~11 Ma and thus could be a much older structure than the other late Cenozoic faults of the Panamint Valley region. The Harrisburg detachment could be related to Late Cretaceous extensional deformation, as observed in the nearby Funeral Mountains (Applegate et al., 1992; Applegate and Hodges, 1995) and from thermochronology data in the Inyo Mountains to the northwest (Lee et al., 2009). Lee et al. (2009) also identified an episode of rapid exhumation in the early Eocene. Mesozoic extensional deformation may have occurred on the Harrisburg detachment portion of the Tucki Mountain detachment system, which would have accommodated some significant fraction of the 22 km of offset of the backfold structure.

The excess values of the previous studies may result from assuming that all of the 22 km of displacement to azimuth 315° on the Tucki Mountain detachment system was ~15 Ma old and younger. If the Harrisburg fault is a pre-Miocene portion of the Tucki Mountain detachment, then the displacement of the Harrisburg fault can be calculated based on our new Miocene displacement data. The offset on the Tucki Mountain detachment is defined by linking features in the Cottonwood Mountains with the northern Panamint Range. Our new results for the Argus Range to Panamint Range slip allow us to calculate a value for the Cottonwood Mountains–Panamint Range slip using the Hunter Mountain fault, which links the Argus Range with the Cottonwood Mountains (Fig. 18). The difference between our vector for the Cottonwood Mountains–Panamint Range displacement and for the Tucki Mountain detachment offset is 14.4 km to 327°, which we would interpret is the slip on the pre-Miocene Harrisburg fault. The azimuth of this result is similar to the west-northwest transport direction azimuth that Hodges et al. (1987) determined for the ductile portion of the Tucki Mountain fault (i.e., the Harrisburg fault) using stretching lineations in the footwall.

Extension, Transtension, and Displacement History

To estimate the displacement history, slip on major faults is interpreted in light of the regional deformation history of roughly west-directed

extension followed by northwest-directed transtension (Snow and Wernicke, 1989; Snow and Lux, 1999; Monastero et al., 2002; Walker et al., 2005; McQuarrie and Wernicke, 2005). The change in the strain fields in the Panamint Valley region has been found to be younger to the west: the Coso region west of Panamint Valley underwent this change ca. 2 Ma ago (Monastero et al., 2002), the Inyo Mountains to the northwest at 2.8 Ma ago (Lee et al., 2009), while the change in Death Valley, to the east, occurred ca. 11 Ma ago (Snow and Wernicke, 1989; Snow and Lux, 1999). Transtension in Panamint Valley was interpreted by Hodges et al. (1989) and Zhang et al. (1990) to have started after the faulted 4.6 Ma old lava flow in northern Panamint Valley (Burchfiel et al., 1987; Sternlof, 1988). Searles Valley, to the west of the Slate Range, may have undergone a change in strain fields ca. 4 Ma ago, based on thermochronology data of Didericksen (2005).

A model for the slip history of Panamint Valley is shown in Figure 19. To obtain the current geologic configuration (Fig. 19A), we superpose a more recent northwest-directed transtension (Fig. 19B) on an initial stage of westward extension (Fig. 19C) using our new displacement constraints. This model has five range blocks bounded by nine faults; all displacements are calculated with respect to the Panamint Range. The main input vectors for this model are given in Table 2 (in bold text). These are the two 15–0 Ma old displacement vectors derived from this study; the 4.2–0 Ma old slip vector on the Hunter Mountain fault (Burchfiel et al., 1987; Sternlof, 1988); and the vectors from Didericksen (2005) for the 15–4.2 Ma old Slate Range detachment and the 4.2–0 Ma old Searles Valley detachment. All other vectors are derived from these.

An important assumption for the Miocene deformation (time 1 in Table 2 and Fig. 19C) is that the Emigrant, Panamint, and Slate Range detachments were a single master normal fault and shared similar slip magnitudes and directions. This assumption is reasonable based on the similar geometries, faulting styles, structural position, and kinematics of these three fault systems and their reconstructed along-strike positions using our new Miocene displacement data. The 4.0 km displacement to an azimuth of 270° (Table 2) used for this episode is derived from a geologic and thermochronologic study by Didericksen (2005) of the exhumation of the southern Slate Range. This number clearly applies to the Slate Range and is consistent with creation of a significant scarp for the Panamint Range and associated deposition of the Miocene Panamint Valley inselberg coarse sedimentary rocks. Slip on the Emigrant fault at this time is consistent

←

Figure 19. Temporal evolution model of Cenozoic displacement in the Panamint Valley region. Simplified geology and fault data modified from Jennings (1977), Moore (1976), Walker et al. (2002), and Didericksen (2005). (A) Geology, structures, and range blocks of Panamint Valley at 0 Ma ago. The five displacement constraints used in the displacement model are shown by the barbell lines (see text and Table 2 for references). (B) Panamint Valley reconstructed to ca. 4.2 Ma ago, based on the displacement model relative to the Panamint Range. Range block displacement vectors are shown for the Cottonwood Mountains (CM), Argus Range (AR), Northern Slate Range (NSR), and southern Slate Range (SRR). Thick dark lines show the active structures during this 4.2–0 Ma ago interval. (C) Panamint Valley reconstructed to ca. 15 Ma ago. This displacement interval is modeled as a 4 km westward displacement of the Argus Range, Cottonwood Mountains, and northern Slate Range in the hanging wall of the Emigrant–Panamint–Slate Range detachment during the interval ca. 15–4.2 Ma ago. The northern Slate Range is outlined in thin black lines so it can be seen where it overlaps the footwall rocks of the Panamint and southern Slate Ranges. Dark gray lines show the reconstructed locations of Mesozoic structures. Note the mismatch of the Independence Dike Swarm between the Argus and Panamint Ranges.

with the geochronologic and stratigraphic work of Snyder and Hodges (2000), although there are no published direct data on the magnitude or direction of motion of this fault at this time. Note that in this model the southern Slate Range remains contiguous with the Panamint Range during Miocene deformation (Fig. 19C).

The Pliocene–Holocene event (time 2 in Table 2) involves distinctly different slip directions for the Argus Range, northern Slate Range, southern Slate Range, and Cottonwood Mountains (Fig. 19B). Thus, time 2 has significant partitioning of slip across the Panamint Valley area, which fits with the work of Walker et al. (2005) and the regional work on slip partitioning of Wesnousky and Jones (1994), Wesnousky (2005), and Le et al. (2007). The only fault in our model that had displacement during both deformation events is the Panamint detachment along the central portion of the western Panamint Range.

This fault slip history model is consistent with most geologic relations around Panamint Valley. We consider, however, the 5 km of displacement on the Towne Pass fault in our model to be slightly problematic. This fault is thought to be a short-lived structure with limited displacement (Snow and Lux, 1999). We propose several possible alternative interpretations. (1) The Emigrant detachment was partially reactivated during time 2 deformation and took up a portion of the 5 km modeled slip of the Towne Pass fault. This explanation agrees with the work of Snow and Lux (1999), but is at odds with the interpretations of Hodges et al. (1989). (2) The numerous faults through Panamint Butte (see Fig. 3 of Burchfiel et al., 1987) accommo-

dated a significant portion of this slip. (3) The Hunter Mountain fault has undergone reactivation of motion in both left-lateral and right-lateral senses (see further discussion). (4) Fault slip increased northward to the Emigrant fault during time 1 deformation. We do not consider this inconsistency for the Towne Pass fault to be a major problem with our study because it is far (>25 km) from the area where our reconstruction data were derived.

Fault Segmentation and Interaction

The Emigrant, Panamint, and Slate Range detachments, interpreted here as a single fault system in the Miocene, initiated as moderate-to high-angle normal faults and were backrotated to lower dips (e.g., McKenna and Hodges, 1990; Snyder and Hodges, 2000; Didericksen, 2005). Subsequently, the Panamint detachment reactivated as a right-lateral oblique normal fault (Cichanski, 2000; Walker et al., 2005); the Slate Range detachment was cut off by a new master normal fault (the Searles Valley fault) and a left-lateral oblique normal fault (Manly Pass fault) (Didericksen, 2005); and the Emigrant detachment was cut by the normal-oblique Towne Pass fault (Hodges et al., 1990; Snyder and Hodges, 2000).

Pliocene–Holocene faulting created a complex pattern of slip partitioning in the Panamint Valley area. The displacement accommodated along the latitude of southern Panamint Valley occurred as north-northwest–striking right-lateral faulting with westward displacement on a north-striking normal fault on the west side

of the southern Slate Range (Fig. 19A). The Panamint detachment accommodated most of the slip in the central portion of Panamint Valley with minor partitioning along the north-northwest–striking, right-lateral Ash Hill fault (Densmore and Anderson, 1997). Slip in the northern Panamint valley was accommodated on the right-lateral Hunter Mountain fault and the Towne Pass normal fault.

The modern Panamint detachment in this model thus appears to end at triple junctions: the right-lateral, northwest-striking Hunter Mountain fault and normal-oblique Towne Pass fault occur at the northern end of the Panamint detachment, and at the southern end there are the right-lateral, north-northwest–striking Southern Panamint Valley fault and the left-lateral normal-oblique Manly Pass fault (Fig. 17A). The southern triple junction is unstable and must migrate northward, elongating the Southern Panamint Valley fault at the expense of the Panamint detachment. This migration effectively partitions the slip accommodated on the Panamint detachment into dominantly dip-slip and strike-slip components that are accommodated on two separate faults. The area to the southeast of the Southern Panamint Valley fault must somehow have accommodated the northward movement of the southern Slate Range, which is bound to the south by the Garlock fault. The southern end of the Slate Range coincides with a bend in the Garlock fault, but the bending does not seem to be enough to accommodate the displacement; therefore, there must also be shortening and vertical-axis rotation of the Owlshhead Mountain east of the Southern Panamint Valley fault, as has

TABLE 2. DISPLACEMENT-TIME MODEL

	Total		Time 1		Time 2	
	Distance (km)	Angle (°)	Distance (km)	Angle (°)	Distance (km)	Angle (°)
2a. Displacement relative to Panamint Range						
Ranges						
Cottonwood Mountains	8.4	295	4.0	270	5.0	314
Argus Range	17.1*	300*	4.0	270	13.8	308
Northern Slate Range	14.7*	296*	4.0	270	11.2	305
Southern Slate Range	10.5	325	0	0	10.5	325
2b. Displacement on specific structures						
Faults						
Emigrant detachment	4.0	270	4.0	270	0	0
Towne Pass fault	5.0	314	0	0	5.0	314
Hunter Mountain fault	8.8	305	0	0	8.8†	305†
Panamint detachment	17.1*	300*	4.0	270	13.8	308
Northern Slate Range faults	2.6	323	0	0	2.6	323
Manly Pass fault	3.8	237	0	0	3.8	237
Southern Panamint Valley fault	10.5	325	0	0	10.5	325
Slate Range detachment	4.0	270	4.0[§]	270[§]	0	0
Searles Valley fault	4.8	270	0	0	4.8[§]	270[§]

Note: The input displacement vectors are denoted by shading and bold type. Time 1: 4.2–15 Ma; Time 2: 0–4.2 Ma ago.

*This study.

†Burchfiel et al. (1987).

§Didericksen (2005).

been found by Serpa and Pavlis (1996), Guest et al. (2003), and Luckow et al. (2005). The northern triple junction is more complicated. The stability of this junction is uncertain, and depends on the amount of obliquity of the Towne Pass fault or any contractional strain along the Hunter Mountain fault (e.g., cf. Dixon et al., 1995, with Oswald and Wesnousky, 2002).

For the central portion of the Panamint detachment to be an active low-angle normal fault, it must somehow be weak, otherwise the slip could be more easily accommodated by higher dip, more strike-slip faulting (Wesnousky and Jones, 1994). The southern and northern ends of the Panamint detachment are abandoning slip on the low-angle detachment fault and partitioning slip into steeper angle faults.

The most obvious factor that could reduce the strength of the Panamint detachment would be the fault gouge developed along it. Numelin et al. (2007b) studied fault gouge from along the central portion of the Panamint detachment. Their friction experiments with these gouge samples showed a relationship of greater total clay content with decreasing friction. Dry samples with 25%–50% clay had coefficients of friction as low as 0.5 at normal stresses equating to ~4.5 km depth using a dip of 20° for the Panamint detachment. Two samples with greater amounts of clay had even lower coefficients of friction of 0.4 for a sample with 57% clay and 0.3 for a sample with 62% clay, for normal stresses equating to ~4.5 km depth. The clays in these fault gouges are dominated by smectite clays. Clay-rich fault gouge can also adsorb water, which reduces the coefficients of friction by 20%–60% (Morrow et al., 2000).

Another explanation for the slip partitioning at the north and south ends of the Panamint detachment would be to look at Panamint Valley as part of the regional slip-partitioning system. The central portion of the Panamint detachment may already be slip partitioned with the higher-angle Sierra Nevada frontal and the Owens Valley faults along the Sierra Nevada (Fig. 1) to the west of Panamint Valley (i.e., Fig. 6 of Wesnousky and Jones, 1994). The results of Lee et al. (2009), however, show that the Panamint detachment could still be the dominant structure in this scenario. Lee et al. (2009) determined that the Hunter Mountain fault, at the northern end of the Panamint detachment, accommodates ~35% of the slip in the Walker Lane, while the faults along the Sierra Nevada accommodate ~10% of the slip. They interpreted that the right-lateral Northern Death Valley fault (Fig. 1) accommodates 45% of the slip, and a fault just east of Death Valley accommodates the last 10%. The geometry and apparent slip partitioning at the northern end of the Panamint detachment might

be influenced by its proximity to the Northern Death Valley fault, whereas the central portion of the Panamint detachment is far enough away to not be as affected. Likewise, the southern end of the Panamint detachment might be influenced by its proximity to the left-lateral Garlock fault (Fig. 1). Both ends of the Panamint detachment might be caught up with the slip on these nearby major faults, pulling the nearby rocks and structures into or with them.

The slip in Death Valley might have behaved in the past in a similar way to modern Panamint Valley, with a central portion of a northward-trending, oblique-slip detachment fault ending to the north and south with dominantly strike-slip faults. The scenario in Death Valley is different today, but it may just be a more advanced version (greater amounts of slip) of the scenario in Panamint Valley today. If this idea holds, then continued transtension in Panamint Valley might link the Hunter Mountain fault with the Southern Death Valley fault, by cutting through the Panamint Range. Thus, the Hunter Mountain fault could eventually resemble the Northern Death Valley fault.

Fault Reactivation

The clearest examples of reactivation in this area are the numerous west-northwest-trending strike-slip faults (Fig. 19A), including the Darwin Tear, Wilson Canyon, and Millspaugh Canyon faults in the Argus Range (Moore, 1976), the New York Canyon fault in the Slate Range (Smith et al., 1968), and several smaller unnamed faults in the Argus, Slate, and Panamint Range (Moore, 1976; Cichanski, 1995; Andrew, 2002). Some of these structures are active in dextral shear today, but most are thought to have been originally left-lateral faults or shear zones (Smith et al., 1968; Moore, 1976; Cichanski, 1995). These west-northwest-striking faults cut Jurassic and Cretaceous rocks in the Argus Range (Moore, 1976; Walker et al., 2002) and thus may be Late Cretaceous in age. They may have developed as conjugates to Late Cretaceous, north-trending, right-lateral shearing found in the Panamint Valley region (Kylander-Clark et al., 2005), or might have been active during latest Jurassic time, accompanying the intrusion of the Independence Dike Swarm (e.g., Carl and Glazner, 2002). This presents the possibility that the similarly oriented Hunter Mountain fault was a preexisting structure that was exploited by the Panamint Valley regional deformation system after the transition to transtensional deformation.

The numerous north-trending, west-dipping faults, such as the Searles Valley, Slate Range, Emigrant, and Tucki Mountain detachments,

may be reactivated Mesozoic thrust and reverse faults, as is apparently the case for at least parts of the Panamint and Searles Valley detachments (Moore, 1976; Fowler, 1982; Andrew, 2002). These Mesozoic fault zones are weaknesses that could be exploited during Miocene east-west extension and the younger northwest-southeast transtension.

A precursor structure of the Southern Panamint Valley fault is not apparent, but it may be a reactivated Mesozoic reverse fault, since the rocks on both sides of southern Panamint Valley between the southern Slate Range and southernmost Panamint Range have numerous examples of Mesozoic eastward contractional deformation (Johnson, 1957; Smith et al., 1968; Andrew, 2002; Dunne and Walker, 2004). In addition, the geology is quite different between the Slate and southern Panamint Ranges, and this mismatch was clearly created prior to the late Cenozoic faulting.

CONCLUSIONS

A Miocene volcanic-sedimentary sequence is preserved in the ranges around the central and southern Panamint Valley. Volcanism occurred ca. 15–13.5 Ma ago. Coarse clastic deposits occur below and are interbedded with the early phase of volcanic rocks (ca. 15 Ma ago), which we interpret to record the initiation of extension in Panamint Valley. A younger, less deformed volcanic episode occurred in the Pliocene, ca. 4.5–4 Ma ago. Post-Pliocene coarse clastic deposits appear to record renewed extension in Panamint Valley.

The Miocene volcanic-sedimentary sequence occurs on either side of Panamint Valley, and we use this to palinspastically reconstruct the extension here. One piercing point uses the unique clast composition of a Miocene boulder to pebble conglomerate in western Panamint Valley to a unique source area in the Panamint Range. This reconstruction vector indicates 17 km of slip on the Panamint detachment fault with an azimuth of 300°. A second slip vector for Panamint Valley aligns the geometry and compositions of the only known Miocene intrusive and/or near-vent facies in the central and southern Panamint Valley area. This reconstructs the northern part of the Slate Range to slightly overlapping the southern Panamint Range with a slip vector of ~15 km to 296° azimuth. A third reconstruction vector was more loosely defined based on Mesozoic intrusive relationships to link the northern and southern Slate Ranges across the Manly Pass fault. This vector was approximately the same as a 9 km westward displacement vector interpreted from thermochronology data in the Slate Range (Didericksen, 2005). We used these reconstruction vectors and the slip vector for the Hunter Mountain fault to calculate the Miocene

and younger displacement of the Cottonwood Mountains from the Panamint Range by 8.4 km to an azimuth of 295°.

Previously published late Cenozoic reconstructions for this region used displacement vectors for the Tucki Mountain detachment to restore Miocene and younger deformation. We consider the ~14 km mismatch of our much shorter Miocene slip vectors compared with the Tucki Mountain detachment slip vector to indicate that part of the Tucki Mountain detachment is older than ~15 Ma. If this is true, then the Harrisburg fault portion of the Tucki Mountain detachment may be similar in age to regionally observed Late Cretaceous (Applegate et al., 1992; Applegate and Hodges, 1995; Lee et al., 2009) or Eocene (Lee et al., 2009) extension.

We created a model of the displacement history of the major detachment faults in Panamint Valley using our new Miocene displacement data in light of the fault geometries, kinematics, and slip constraints of previous studies (Burchfiel et al., 1987; Didericksen, 2005; Walker et al., 2005). We model the ~15 Ma old extension to have occurred on a single detachment fault that is now broken up into the Emigrant, Panamint, and Slate Range detachments. A second phase of extension occurred during the Pliocene–Holocene with extension axes oblique to the earlier deformation. The earlier detachment faults are partially reactivated, and a system of strike-slip and oblique normal faults modifies the earlier detachment faults. Slip in central Panamint Valley is accommodated by right-lateral, oblique normal slip on the reactivated low-angle Panamint detachment. Farther north, the Panamint detachment ends and forms a triple point with the Hunter Mountain and Towne Pass faults. The southern end of the Panamint detachment also ends at a triple point with the Manly Pass fault and the Southern Panamint Valley fault. This geometry of the southern triple point is unstable and it must migrate northward.

The continued oblique slip on the low-angle Panamint detachment fault is puzzling, because slip would more easily be partitioned onto regional high-angle faults (Wesnousky and Jones, 1994; Lee et al., 2007). One possibility is that the Panamint detachment is exceptionally weak. Numelin et al. (2007b) measured the friction values of fault gouges along the Panamint detachment and found that some of the gouge samples were very clay rich and had low friction coefficients. The presence of this weak fault gouge along the Panamint detachment may explain its continued slip under otherwise unfavorable conditions.

The complicated geometry and kinematics of the slip partitioning in Panamint Valley may be also explained by the close proximity of the

Northern Death Valley and Garlock faults, which could be dragging the northern and southern ends of the Panamint Valley system with them. It is clear that older structures play a fundamental role in controlling some Pliocene and younger deformation. This reactivation of structures may be more conspicuous in Panamint Valley because of the relatively immature fault system of the Walker Lane. The complicated geometries and kinematics of faulting in Panamint Valley may eventually be erased as more slip accumulates and fault links develop more to create a through-going fault zone (Wesnousky, 2005).

ACKNOWLEDGMENTS

Reviews by R. Keller, C. Jones, Jon Spencer, and an anonymous reviewer greatly improved this manuscript. This study was partially supported by grants awarded to Walker from the Geothermal Program Office at China Lake Naval Weapons Station and the EarthScope Program of the National Science Foundation. We are indebted to discussions with numerous researchers on the geology of the Panamint Valley Region, including George Dunne, Frank Monastero, Jon Spencer, Brad Didericksen, Eric Kirby, Terry Pavlis, and Marek Cichanski.

REFERENCES CITED

- Albee, A.L., Labotka, T.C., Lanphere, M.A., and McDowell, S.D., 1981, Geologic map of the Telescope Peak Quadrangle, California: U.S. Geological Survey Geologic Quadrangle map GQ-1532, scale 1:62,500.
- Andrew, J.E., 2002, The Mesozoic and Tertiary tectonic history of the Panamint Range and Quail Mountains, California [Ph.D. thesis]: Lawrence, University of Kansas, 154 p.
- Applegate, J.D.R., and Hodges, K.V., 1995, Mesozoic and Cenozoic extension recorded by metamorphic rocks in the Funeral Mountains, California: Geological Society of America Bulletin, v. 107, p. 1063–1076, doi: 10.1130/0016-7606(1995)107<1063:MACERB>2.3.CO;2.
- Applegate, J.D.R., Walker, J.D., and Hodges, K.V., 1992, Late Cretaceous extensional unroofing in the Funeral Mountains metamorphic core complex, California: Geology, v. 20, p. 519–522, doi: 10.1130/0091-7613(1992)020<0519:LCEUT>2.3.CO;2.
- Bruesseke, M.E., Hart, W.K., and Heizler, M.T., 2007, Diverse mid-Miocene silicic volcanism associated with the Yellowstone–Newberry thermal anomaly: Journal of Volcanology and Geothermal Research, v. 161, p. 187–214, doi: 10.1016/j.jvolgeores.2006.12.004.
- Burchfiel, B.C., and Stewart, J.H., 1966, Pull-apart origin of the central segment of Death Valley, California: Geological Society of America Bulletin, v. 77, p. 439–441, doi: 10.1130/0016-7606(1966)77[439:POOTCS]2.0.CO;2.
- Burchfiel, B.C., Hodges, K.V., and Royden, L.H., 1987, Geology of Panamint Valley–Saline Valley pull-apart system, California: palimpsestic evidence for low-angle geometry of a Neogene range-bounding fault: Journal of Geophysical Research, v. 92, no. B10, p. 10,422–10,426, doi: 10.1029/JB092iB10p10422.
- Carl, B.S., and Glazner, A.F., 2002, Extent and significance of the Independence dike swarm, eastern California, in Glazner, A.F., et al., eds., Geologic evolution of the Mojave Desert and Southwestern Basin and Range: Geological Society of America Memoir 195, p. 117–130.
- Chen, J.H., and Moore, J.G., 1979, Late Jurassic Independence dike swarm in eastern California: Geology, v. 7, p. 129–133, doi: 10.1130/0091-7613(1979)7<129:LJIDS>2.0.CO;2.
- Cichanski, M.A., 1995, Tectonic evolution of a portion of the Panamint Mountains, Death Valley, California [Ph.D. thesis]: Los Angeles, University of Southern California, 321 p.
- Cichanski, M.A., 2000, Low-angle, range-flank faults in the Panamint, Inyo, and Slate Ranges, California: implications for recent tectonics of the Death Valley region: Geological Society of America Bulletin, v. 112, p. 871–883, doi: 10.1130/0016-7606(2000)112<0871:LARFFI>2.3.CO;2.
- Densmore, A.L., and Anderson, R.S., 1997, Tectonic morphology of the Ash Hill fault, Panamint Valley, California: Basin Research, v. 9, p. 53–63, doi: 10.1046/j.1365-2117.1997.00028.x.
- Didericksen, B., 2005, Middle Miocene to recent faulting and exhumation of the central Slate Range, Eastern California Shear Zone [M.S. thesis]: Lawrence, University of Kansas, 104 p.
- Dixon, T.H., Robaudo, S., Lee, J., and Reheis, M.C., 1995, Constraints on present-day Basin and Range deformation from space geodesy: Tectonics, v. 14, p. 755–772, doi: 10.1029/95TC00931.
- Dixon, T.H., Miller, M., Farina, F., Wang, H., and Johnson, D., 2000, Present-day motion of the Sierra Nevada block and some tectonic implications for the Basin and Range Province, North America Cordillera: Tectonics, v. 19, p. 1–24, doi: 10.1029/1998TC001088.
- Dokka, R.K., and Travis, C.J., 1990, Role of the Eastern California Shear Zone in accommodating Pacific–North America plate motion: Geophysical Research Letters, v. 17, p. 1323–1326, doi: 10.1029/GL017i009p01323.
- Dunne, G.C., and Walker, J.D., 1993, Age of Jurassic volcanism and tectonism, southern Owens Valley region, east-central California: Geological Society of America Bulletin, v. 105, p. 1223–1230, doi: 10.1130/0016-7606(1993)105<1223:AOJVAT>2.3.CO;2.
- Dunne, G.C., and Walker, J.D., 2004, Structure and evolution of the East Sierran thrust system, east-central California: Tectonics, v. 23, TC4012, doi: 10.1029/2002TC001478.
- Fowler, J.A., 1982, Structural analysis of Mesozoic deformation in the central Slate Range, eastern California [M.S. thesis]: Northridge, California State University, 135 p.
- Guest, B., Pavlis, T.L., Golding, H., and Serpa, L., 2003, Chasing the Garlock: A study of tectonic response to vertical axis rotation: Geology, v. 31, p. 553–556, doi: 10.1130/0091-7613(2003)031<0553:CTGASO>2.0.CO;2.
- Hall, W.E., 1971, Geology of the Panamint Butte Quadrangle, Inyo County, California: U.S. Geological Survey Bulletin 1299, 67 p.
- Hodges, K.V., and Walker, J.D., 1990, Petrologic constraints on the unroofing history of the Funeral Mountains metamorphic core complex, California: Journal of Geophysical Research, v. 95, p. 8437–8445, doi: 10.1029/JB095iB06p08437.
- Hodges, K.V., Walker, J.D., and Wernicke, B.P., 1987, Footwall structural evolution of the Tucki Mountain detachment system, Death Valley region, southeastern California, in Coward, M.P., et al., eds., Continental extensional tectonics: Geological Society of London Special Publication 28, p. 393–408.
- Hodges, K.V., McKenna, L.W., Stock, J.M., Knapp, J.H., and Walker, J.D., 1989, Structural relationships between Neogene extensional basins, Panamint Valley area, southeast California: New perspectives of Basin and Range topography: Tectonics, v. 8, p. 453–467, doi: 10.1029/TC008i003p00453.
- Hodges, K.V., McKenna, L.W., and Harding, M.B., 1990, Structural unroofing of the central Panamint Mountains, Death Valley region, southeastern California, in Wernicke, B.P., ed., Basin and Range extensional tectonics near the latitude of Las Vegas, Nevada: Geological Society of America Memoir 176, p. 377–390.
- Hopper, R.H., 1947, Geologic section from the Sierra Nevada to Death Valley, California: Geological Society of America Bulletin, v. 58, p. 393–432, doi: 10.1130/0016-7606(1947)58[393:GSFTSN]2.0.CO;2.
- House, M.A., Bowring, S.A., and Hodges, K.V., 2002, Implications of middle Eocene epizonal plutonism for the unroofing history of the Bitterroot metamorphic

Reconstructing late Cenozoic deformation in central Panamint Valley

- core complex, Idaho-Montana: Geological Society of America Bulletin, v. 114, p. 448–461, doi: 10.1130/0016-7606(2002)114<0448:IOMEEP>2.0.CO;2.
- Jennings, C.W., 1977, Geologic map of California: California Division of Mines and Geology, California Geological Data Map Series Map no. 2, scale 1:750,000.
- Jennings, C.W., Burnett, J.L., and Troxel, B.W., 1962, Geologic map of California; Trona sheet: California Division of Mines and Geology, scale 1:250,000.
- Johnson, B.K., 1957, Geology of a part of the Manly Peak Quadrangle, southern Panamint Range, California: University of California Publications in Geological Sciences, v. 30, p. 353–423.
- Kirby, E., Gosse, J., McDonald, E., and Walker, J.D., 2004, Late Quaternary–recent slip on a low-angle normal fault; inferences from alluvial deposits along the Panamint Valley fault system: Geological Society of America Abstracts with Programs, v. 36, no. 5, p. 547.
- Kylander-Clark, A.R.C., Coleman, D.S., Glazner, A.F., and Bartley, J.M., 2005, Evidence for 65 km of dextral slip across Owens Valley, California, since 83 Ma: Geological Society of America Bulletin, v. 117, p. 962–968, doi: 10.1130/B25624.1.
- Labotka, T.C., Albee, A.L., Lanphere, M.A., and McDowell, S.D., 1980, Stratigraphy, structure, and metamorphism in the central Panamint Mountains (Telescope Peak Quadrangle), Death Valley area, California: Geological Society of America Bulletin, v. 91, p. I25–I129, I1843–I1933.
- Lee, K., Lee, J., Owen, O., and Finkel, R., 2007, Late Quaternary slip rates along the Sierra Nevada frontal fault zone, California: Slip partitioning across the western margin of the Eastern California Shear Zone–Basin and Range Province: Geological Society of America Bulletin, v. 119, p. 240–256, doi: 10.1130/B25960.1.
- Lee, J., Stockli, D.F., Owen, L.A., Finkel, R.C., and Kislit-syn, R., 2009, Exhumation of the Inyo Mountains, California: Implications for the timing of extension along the western boundary of the Basin and Range Province and distribution of dextral fault slip rates across the eastern California shear zone: Tectonics, v. 28, TC1001, doi: 10.1029/2008TC002295.
- Luckow, H.G., Pavlis, T.P., Serpa, L.F., Guest, B., Wagner, D.L., Snee, L., Hensley, T., and Korjenkova, A., 2005, Late Cenozoic sedimentation and volcanism during transtensional deformation in Wingate Wash and the Owlshad Mountains, Death Valley: Earth-Science Reviews, v. 73, p. 177–219, doi: 10.1016/j.earscirev.2005.07.013.
- Mahood, G.A., Nibler, G.E., and Halliday, A.N., 1996, Zoning patterns and petrologic processes in peraluminous magma chambers; Hall Canyon Pluton, Panamint Range, California: Geological Society of America Bulletin, v. 108, p. 437–453, doi: 10.1130/0016-7606(1996)108<0437:ZPAPPI>2.3.CO;2.
- Maxson, J.H., 1950, Physiographic features of the Panamint Range, California: Geological Society of America Bulletin, v. 61, p. 99–114, doi: 10.1130/0016-7606(1950)61[99:PFOTPR]2.0.CO;2.
- McKenna, L.W., and Hodges, K.V., 1990, Constraints on the kinematics and timing of late Miocene–recent extension between the Panamint and Black Mountains, southeastern California, in Wernicke, B.P., ed., Basin and Range extensional tectonics near the latitude of Las Vegas, Nevada: Geological Society of America Memoir 176, p. 363–376.
- McQuarrie, N., and Wernicke, B., 2005, An animated tectonic reconstruction of southwestern North America since 36 Ma: Geosphere, v. 1, no. 3, p. 147–172, doi: 10.1130/GES00016.1.
- Monastero, F.C., Katzenstein, A.M., Walker, J.D., and Sabin, A.E., 2002, Neogene evolution of the Indian Wells Valley, east-central California, in Glazner, A.F., and Walker, J.D., eds., Geologic evolution of the central Mojave Desert and Southern Basin and Range: Geological Society of America Memoir 19, p. 199–228.
- Moore, S.C., 1976, Geology and thrust fault tectonics of parts of the Argus and Slate ranges, Inyo County, California [Ph.D. thesis]: Seattle, University of Washington, 127 p.
- Morrow, C.A., Moore, D.E., and Lockner, D.A., 2000, The effect of mineral bond strength and adsorbed water on fault gouge frictional strength: Geophysical Research Letters, v. 27, p. 815–818, doi: 10.1029/1999GL008401.
- Numelin, T., Didericksen, B., Kirby, E., and Walker, J.D., 2007a, Late Pleistocene slip on a low-angle normal fault, Searles Valley, California: Geosphere, v. 3, no. 3, p. 163–176, doi: 10.1130/GES00052.1.
- Numelin, T., Marone, C., and Kirby, E., 2007b, Frictional properties of natural fault gouge from a low-angle normal fault, Panamint Valley, California: Tectonics, v. 26, TC2004, doi: 10.1029/2005TC001916.
- Oldow, J.S., 1992, Late Cenozoic displacement partitioning in the northwestern Great Basin, in Craig, S.D., ed., Walker Lane symposium: Structure, tectonics and mineralization of the Walker Lane: Reno, Geological Society of Nevada, p. 17–52.
- Oswald, J.A., and Wesnousky, S.G., 2002, Neotectonics and Quaternary geology of the Hunter Mountain fault zone and Saline Valley region, southeastern California: Geomorphology, v. 42, p. 255–278, doi: 10.1016/S0169-555X(01)00089-7.
- Prave, A.R., and Wright, L.A., 1986, Isopach pattern of the Lower Cambrian Zabriskie Quartzite, Death Valley region, California–Nevada; how useful in tectonic reconstructions?: Geology, v. 14, p. 251–254, doi: 10.1130/0091-7613(1986)14<251:IPOTLCS>2.0.CO;2.
- Schweig, E.S., III, 1989, Basin-range tectonics in the Darwin Plateau, southwestern Great Basin, California: Geological Society of America Bulletin, v. 101, p. 652–662, doi: 10.1130/0016-7606(1989)101<0652:BRITTD>2.3.CO;2.
- Serpa, L., and Pavlis, T.L., 1996, Three-dimensional model of the Cenozoic history of the Death Valley region, southeastern California: Tectonics, v. 15, no. 6, p. 1113–1128, doi: 10.1029/96TC01633.
- Smith, G.I., Troxel, B.W., Gray, C.H., and von Huene, R., 1968, Geologic reconnaissance of the Slate Range, San Bernardino and Inyo counties, California: California Division of Mines and Geology Special Report 96, 33 p.
- Smith, R.S.U., 1979, Holocene offset and seismicity along the Panamint Valley fault zone, western Basin-and-Range Province, California: Tectonophysics, v. 52, p. 411–415, doi: 10.1016/0040-1951(79)90256-7.
- Snow, J.K., and Lux, D.R., 1999, Tectono-sequence stratigraphy of Tertiary rocks in the Cottonwood Mountains and northern Death Valley area, California and Nevada, in Troxel, B.W., ed., Cenozoic basins of the Death Valley region: Geological Society of America Special Paper 333, p. 17–64.
- Snow, J.K., and Wernicke, B.P., 1989, Uniqueness of geologic correlations; an example from the Death Valley extended terrain: Geological Society of America Bulletin, v. 101, p. 1351–1362, doi: 10.1130/0016-7606(1989)101<1351:UOGCAE>2.3.CO;2.
- Snow, J.K., and Wernicke, B.P., 2000, Cenozoic tectonism in the central Basin and Range: Magnitude, rate and distribution of upper crustal strain: American Journal of Science, v. 300, p. 659–719, doi: 10.2475/ajs.300.9.659.
- Snyder, N.P., and Hodges, K.V., 2000, Depositional and tectonic evolution of a supradetachment basin: ⁴⁰Ar/³⁹Ar geochronology of the Nova Formation, Panamint Range, California: Basin Research, v. 12, p. 19–30, doi: 10.1046/j.1365-2117.2000.00108.x.
- Sternlof, K.R., 1988, Structural style and kinematic history of the active Panamint–Saline extensional system, Inyo County, California [M.S. thesis]: Cambridge, Massachusetts Institute of Technology, 40 p.
- Stewart, J.H., 1980, Geology of Nevada: a discussion to accompany the Geologic Map of Nevada: Nevada Bureau of Mines and Geology Special Publication, n. 4, 136 p.
- Stewart, J.H., 1983, Extensional tectonics in the Death Valley area, California: Transport of the Panamint Range structural block 80 km northwestward: Geology, v. 11, p. 153–157, doi: 10.1130/0091-7613(1983)11<153:ETITDV>2.0.CO;2.
- Stone, P., 1985, Stratigraphy, depositional history, and paleogeographic significance of Pennsylvanian and Permian rocks in the Owens Valley–Death Valley region, California [Ph.D. thesis]: Stanford University, 470 p.
- Vogel, M.B., Jayko, A.S., Smith, R.S.U., and Wooden, J.L., 2002, Quaternary exhumation rate central Panamint Range, California from U–Pb zircon ages: Geological Society of America Abstracts with Programs, v. 34, no. 6, p. 249.
- Wagner, D.L., 1988, Evidence for late Cenozoic extension across Wingate Wash, Death Valley region, southeastern California, in Gregory, J.L., and Baldwin, E.J., eds., Geology of the Death Valley region: South Coast Geological Society Annual field Trip Guidebook, no. 16, p. 243–259.
- Walker, J.D., and Black, R.A., 2000, Mapping the outcrop: Geotimes, v. 45, no. 11, p. 28–31.
- Walker, J.D., Black, R.A., Linn, J.K., Thomas, A.J., Wiseman, R., and D’Attilio, M.G., 1996, Development of geographic information systems-oriented databases for integrated geological and geophysical applications: GSA Today, v. 6, no. 3, p. 1–7.
- Walker, J.D., Berry, A.K., Davis, P.J., Andrew, J.E., and Mitsdarfer, J.M., 2002, Geologic map of the northern Mojave Desert and southwestern Basin and Range Province, California, in Glazner, A.F., et al., eds., Geological evolution of the Mojave Desert and Southwestern Basin and Range: Geological Society of America Memoir 195, scale 1:250,000.
- Walker, J.D., Andrew, J.E., and Kirby, E., 2005, Strain transfer and partitioning between the Panamint Valley, Searles Valley, and Ash Hill fault zones, California: Geosphere, v. 1, no. 3, p. 111–118, doi: 10.1130/GES00014.1.
- Wernicke, B., 1985, Uniform-sense normal simple shear of the continental lithosphere: Canadian Journal of Earth Sciences, v. 22, p. 108–125.
- Wernicke, B., Axen, G.J., and Snow, J.K., 1988, Basin and Range extensional tectonics at the latitude of Las Vegas, Nevada: Geological Society of America Bulletin, v. 100, p. 1738–1757, doi: 10.1130/0016-7606(1988)100<1738:BARETA>2.3.CO;2.
- Wernicke, B., Spencer, J.E., Burchfiel, B.C., and Guth, P.L., 1982, Magnitude of crustal extension in the southern Great Basin: Geology, v. 10, p. 499–502, doi: 10.1130/0091-7613(1982)10<499:MOCEIT>2.0.CO;2.
- Wernicke, B., Walker, J.D., and Hodges, K.V., 1986, Geologic evolution of Tucki Mountain and vicinity, central Panamint Range, in Dunne, G.C., ed., Mesozoic–Cenozoic structural evolution of selected areas, east-central California: Geological Society of America Cordilleran Section, Field Trip 2 Guidebook, p. 67–80.
- Wesnousky, S.G., 2005, Active faulting in the Walker Lane: Tectonics, v. 24, TC3009, doi: 10.1029/2004TC001645.
- Wesnousky, S.G., and Jones, C.H., 1994, Slip partitioning, spatial and temporal changes in the regional stress field, and the relative strength of active faults in the Basin and Range: Geology, v. 22, p. 1031–1034, doi: 10.1130/0091-7613(1994)022<1031:OSSPSA>2.3.CO;2.
- Wright, L., 1976, Late Cenozoic fault patterns and stress fields in the Great Basin and westward displacement of the Sierra Nevada block: Geology, v. 4, p. 489–494, doi: 10.1130/0091-7613(1976)4<489:LCPAS>2.0.CO;2.
- Wrucke, C.T., Stevens, C.H., and Wooden, J.L., 1995, The Butte Valley and Layton Well thrusts of eastern California; distribution and regional significance: Tectonics, v. 14, no. 5, p. 1165–1171, doi: 10.1029/95TC01932.
- Zhang, P., Ellis, M., Stemmmons, D.B., and Mao, F., 1990, Right-lateral displacements and the Holocene slip rate associated with prehistoric earthquakes along the southern Panamint Valley fault zone; implications for southern Basin and Range tectonics and coastal California deformation: Journal of Geophysical Research, v. 95, p. 4857–4872, doi: 10.1029/JB095I04p04857.

MANUSCRIPT RECEIVED 1 APRIL 2008
 REVISED MANUSCRIPT RECEIVED 29 JANUARY 2009
 MANUSCRIPT ACCEPTED 9 MARCH 2009